JCI insight

Fibulin-1c regulates transforming growth factor-β activation in pulmonary tissue fibrosis

Gang Liu, … , Janette K. Burgess, Philip M. Hansbro

JCI Insight. 2019. https://doi.org/10.1172/jci.insight.124529.

Research In-Press Preview **Cell biology** **Immunology**

Tissue remodeling/fibrosis is a major feature of all fibrotic diseases, including idiopathic pulmonary fibrosis (IPF). It is underpinned by accumulating extracellular matrix (ECM) proteins. Fibulin-1c (Fbln1c) is a matricellular ECM protein associated with lung fibrosis in both humans and mice, and stabilizes collagen formation. Here we discovered that Fbln1c was increased in the lung tissues of IPF patients and experimental bleomycin-induced pulmonary fibrosis. *Fbln1c*-deficient ($^{-/-}$) mice had reduced pulmonary remodeling/fibrosis and improved lung function after bleomycin challenge. Fbln1c interacted with fibronectin, periostin and tenascin-c in collagen deposits following bleomycin challenge. In a novel mechanism of fibrosis Fbln1c bound to latent transforming growth factor (TGF)-β binding protein-1 (LTBP1) to induce TGF-β activation, and mediated downstream Smad3 phosphorylation/signaling. This process increased myofibroblast numbers and collagen deposition. Fbln1 and LTBP1 co-localized in lung tissues from IPF patients. Thus, Fbln1c may be a novel driver of TGF-β-induced fibrosis involving LTBP1 and may be an upstream therapeutic target.

RESEARCH ARTICLE

Fibulin-1c regulates transforming growth factor-β activation in pulmonary tissue fibrosis

Gang Liu,[1,2,3] Marion A. Cooley,[4] Andrew G. Jarnicki,[1,5] Theo Borghuis,[6] Prema M. Nair,[1] Gavin Tjin,[7] Alan C. Hsu,[1] Tatt Jhong Haw,[1] Michael Fricker,[1] Celeste L. Harrison,[1] Bernadette Jones,[1] Nicole G. Hansbro,[1,2,3] Peter A. Wark,[1] Jay C. Horvat,[1] W. Scott Argraves,[4] Brian G. Oliver,[2,7] Darryl A. Knight,[1] Janette K. Burgess,[6,7] and Philip M. Hansbro[1,2,3]

Affiliations

[1]Priority Research Centre for Healthy Lungs, Hunter Medical Research Institute and The University of Newcastle, Newcastle, New South Wales, Australia

[2]School of Life Sciences, University of Technology Sydney, Sydney, New South Wales, Australia

[3]Centenary Institute, Sydney, New South Wales, Australia

[4]Department of Oral Biology and Diagnostic Sciences, Augusta University, Augusta, Georgia, USA;

[5]Department of Pharmacology and Therapeutics, University of Melbourne, Parkville, Victoria, Australia

[6]University of Groningen, University Medical Center Groningen, Groningen Research Institute for Asthma and COPD (GRIAC), Department of Pathology and Medical Biology, Groningen, The Netherlands

[7]Woolcock Institute of Medical Research, Discipline of Pharmacology, The University of Sydney, Sydney, New South Wales, Australia

Corresponding authors

Correspondence to Philip M. Hansbro: Philip.Hansbro@uts.edu.au

Conflict of Interest

The authors have declared that no conflict of interest exists

Max 9,000 words, current 5,689 words

Abstract word count: limit 200 words, current 155

Abstract

Tissue remodeling/fibrosis is a major feature of all fibrotic diseases, including idiopathic pulmonary fibrosis (IPF). It is underpinned by accumulating extracellular matrix (ECM) proteins. Fibulin-1c (Fbln1c) is a matricellular ECM protein associated with lung fibrosis in both humans and mice, and stabilizes collagen formation. Here we discovered that Fbln1c was increased in the lung tissues of IPF patients and experimental bleomycin-induced pulmonary fibrosis. *Fbln1c*-deficient ($^{-/-}$) mice had reduced pulmonary remodeling/fibrosis and improved lung function after bleomycin challenge. Fbln1c interacted with fibronectin, periostin and tenascin-c in collagen deposits following bleomycin challenge. In a novel mechanism of fibrosis Fbln1c bound to latent transforming growth factor (TGF)-β binding protein-1 (LTBP1) to induce TGF-β activation, and mediated downstream Smad3 phosphorylation/signaling. This process increased myofibroblast numbers and collagen deposition. Fbln1 and LTBP1 co-localized in lung tissues from IPF patients. Thus, Fbln1c may be a novel driver of TGF-β-induced fibrosis involving LTBP1 and may be an upstream therapeutic target.

Introduction

Tissue remodeling and fibrosis are major features of fibrotic diseases, including those affecting the lung, such as idiopathic pulmonary fibrosis (IPF) (1, 2). Fibrosis results from the excessive tissue deposition of extracellular matrix (ECM) proteins produced predominantly from myofibroblasts, which leads to increased collagen deposition in tissues(3). Multiple ECM proteins are involved in fibrosis, including collagens, fibronectin (Fn), periostin (Postn) and tenasin-c (Tnc) (3-5). The mechanisms that drive fibrosis involve transforming growth factor (TGF)-β mediated pathways (6) but how these are induced remains incompletely understood.

IPF is a chronic, progressive, and lethal interstitial fibrotic lung disease that primarily occurs in older adults (7). Its prognosis is poor with an average survival of 2-3 years after diagnosis, lower than most cancers (7, 8). IPF is characterized by dyspnoea, dry cough, and progressive airway and lung tissue remodeling (9). IPF patients have increased collagen deposition around the small airways (10) and interstitial and airspace fibrosis of the lung parenchyma (11). This leads to reduced lung function, including a decline in forced vital capacity that accompanies disease progression (12). The cause of IPF is unknown, however cigarette smoke, environmental insults and genetic predisposition are primary etiological factors (13, 14) and (TGF)-β mediated pathways and downstream Smad signal transducers are well known to be involved (6). Current therapies directly target the tissue remodeling in IPF but have limited efficacy. Nintedanib targets multiple receptors and tyrosine kinases and slows disease progression in IPF patients (15). Pirfenidone, an anti-fibrotic drug, downregulates the production of TGF-β and suppresses the progression of pulmonary fibrosis (6). Both drugs delay the impairment of lung function and improve the survival

rate of IPF patients (6, 15). However, these treatments are not cures, often have debilitating side-effects, and delay rather than inhibit or reverse pulmonary remodeling.

Fibulin-1 (Fbln1), a secreted glycoprotein, is an important matricellular ECM protein (16). It facilitates the stabilization and binding of other ECM proteins, such as Fn, Postn, Tnc and versican during collagen deposition (1). There are four Fbln1 variants (Fbln1a, b, c and d) in humans that differ in their C-terminal sequences, but only Fbln1c and d occur in mice (17). Fbln1c is the variant that is associated with respiratory diseases in humans and mice (1, 18). We previously showed that Fbln1 protein levels are increased in serum/plasma and lung tissue from patients with IPF (18), however, the level of the Fbln1c variant was not assessed. We also showed that a Fbln1c peptide increases the proliferation of lung fibroblasts from IPF patients (19), and that *Fbln1c*-deficient ($^{-/-}$) mice are protected against bleomycin-induced small airway remodeling (1). We also showed similar roles for Fbln1c in fibrosis in chronic obstructive pulmonary disease (COPD) and asthma (1, 20). However, the roles of Fbln1c in pulmonary fibrosis and the mechanisms involved remain unknown.

In this study, we show that Fbln1c levels are increased in the lung tissues of IPF patients and demonstrate that it is essential for the development of experimental model of pulmonary fibrosis. Inhibition of *Fbln1c* in mice are protected from developing airway and lung remodeling/fibrosis through the attenuation of the TGF-β signaling pathway and myofibroblast generation. We identify a novel mechanism that involves Fbln1c binding to LTBP1 to activate the TGF-β signaling pathway to induce fibrosis. These data increase fundamental understanding of development of fibrosis and Fbln1c may drive TGF-β activation and signaling and be a potential upstream therapeutic target in IPF and other fibrotic diseases.

Results

Fbln1 levels are increased in the lung tissues of IPF patients. To understand role of Fbln1c in fibrosis, we used IPF, one of severe fibrotic diseases (9) as an example. Lung tissues were obtained from IPF patients and controls with normal lungs (Table 1). Fbln1c protein levels, measured by immunohistochemistry, were significantly increased specifically in fibrotic areas of the lungs from IPF patients, but not in non-fibrotic areas or in the lungs from controls (Figure 1A).

Fbln1c is increased around small airways and in lungs in experimental bleomycin-induced pulmonary fibrosis. In order to determine the role of Fbln1c in pulmonary fibrosis, a previously described experimental model of bleomycin-induced lung fibrosis was used (21-23). One dose of bleomycin was administered (0.05U, intranasally) and collagen deposition around the small airways and in lungs was assessed after 7, 14, 21, and 28 days. Bleomycin challenge significantly induced deposition of collagen around the small airways after 21 days, which increased further after 28 days, compared with sham-challenged controls (Figure 1B and Supplementary; supplemental material available online with this article). Concomitant with this, there were also significant increases in the levels of total lung hydroxyproline, a surrogate marker for elevated total collagen levels, following bleomycin challenge, in whole lung tissues after 28 days (Supplementary Figure 1).

We then measured Fbln1 protein levels around the airways and in whole lung tissues over the 28-day time-course after bleomycin challenge using immunohistochemistry. Fbln1 deposition around the small airways was significantly increased from 14 days, compared with sham-challenged controls (Figure 1B and Supplementary Figure 2). Fbln1 protein levels in whole lung tissues assessed using

immunoblotting were also significantly increased following bleomycin exposure after 21 and 28 days (Figure 1C).

Lung fibrosis was maximally increased around the airways and in the lungs after 28 days, thus we measured Fbln1c specific protein levels in mouse lung sections at this time-point. Deposition of Fbln1c was significantly increased around the small airways (Figure 1D) and in the parenchyma (Figure 1E) 28 days after bleomycin challenge, and the Fbln1c protein levels were also increased in whole lung tissue (Figure 1F). The levels of increased Fbln1 and Fbln1c in mice treated with 28 days bleomycin challenge are similar, indicating that Fbln1c plays key roles in lung fibrosis compared to Fbln1d.

Genetic deletion of Fbln1c protects against experimental bleomycin-induced pulmonary fibrosis. The 28-day time point after bleomycin treatment was also used to assess the effect of Fbln1c deficiency. Deletion of all *Fbln1* isoforms in mice is embryonically lethal, thus *Fbln1c*$^{-/-}$ mice were created and used(1). *Fbln1c* mRNA levels were significantly increased in wild-type (WT) mouse lungs 28 days after bleomycin challenge, but were undetectable in *Fbln1c*$^{-/-}$ mice (Figure 2A). However, *Fbln1d* mRNA levels in WT and *Fbln1c*$^{-/-}$ mice were not altered (Figure 2B). The absence of *Fbln1c* completely inhibited the development of bleomycin-induced collagen deposition around the small airways compared to WT mice (Figure 2C), congruent with our previous findings in COPD(1). In addition, *Fbln1c* deficiency completely prevented increases in total and soluble collagen levels (Figure 2D), and in type I collagen-α1 (Col1a1), the most abundant collagen in diseased lungs, in whole lung tissues (Figure 2, E–F).

Second harmonic generation (SHG) microscopy has been recently used as a powerful and robust tool to visualize changes in collagen microstructure in tissues (24, 25). SHG emits two-photon scattering in the focal volume, forwards (F_{SHG}) and backwards (B_{SHG}), and the F_{SHG}/B_{SHG} relationship is sensitive to the spatial extent of SHG-generated scattering to indicate the disorder of arrangement and density of collagen fibrils. The ratio of F_{SHG}/B_{SHG} area was significantly increased in WT mice 28 days after bleomycin challenge compared with controls (Figure 2G and Supplementary Figure 3). Again, *Fbln1c*$^{-/-}$ mice were protected against this increase.

The balance of matrix metalloproteinase (MMP) and tissue inhibitor of metalloproteinase (TIMP) regulates ECM protein production (1). Thus, we then measured the mRNA levels of these proteins in the lungs from WT and *Fbln1c*$^{-/-}$ mice. Bleomycin-challenged WT mice had substantial increases in the mRNA levels of *Mmp1*, 3, 8, 12, and 13 in lung tissues after 28 days compared with controls (Supplementary Figure 4, A–E). These increases were abrogated in *Fbln1c*$^{-/-}$ mice. The mRNA levels of *Timp1* were also increased in bleomycin-challenged WT mice, but not *Fbln1c*$^{-/-}$ mice (Supplementary Figure 4F).

To determine whether protection against pathological changes in *Fbln1c*$^{-/-}$ mice prevented functional changes, lung function parameters were assessed in WT and *Fbln1c*$^{-/-}$ mice 28 days after bleomycin challenge. Bleomycin challenge increased tissue damping and tissue elastance, and reduced lung compliance in WT mice, but *Fbln1c*$^{-/-}$ mice were protected against these changes (Figure 2, H–J).

Fbln1c deficiency protects against bleomycin-induced accumulation of Fn and Tnc around the small airways and in whole lung tissues. Fbln1 is critical for ECM stabilization (1), thus we next assessed the specific role of Fbln1c in the deposition of

ECM and remodeling around the small airways in bleomycin-induced pulmonary fibrosis. Bleomycin challenge induced Fn and Tnc deposition in the basement membrane around the small airways after 28 days in WT mice (Figure 3, A and B). Again, *Fbln1c*$^{-/-}$ mice were protected against these changes. In contrast, Postn deposition was not altered in WT or *Fbln1c*$^{-/-}$ mice (Figure 3C).

We then assessed the role of Fbln1c in ECM protein deposition in whole lung tissues. Bleomycin challenge substantially increased *Fn* and *Tnc* mRNA levels in WT mouse lungs, whereas *Fbln1c*$^{-/-}$ mice were protected (Figure 3, D and E). *Postn* mRNA levels in lungs were not altered in WT or *Fbln1c*$^{-/-}$ mice after bleomycin challenge (Figure 3F). Bleomycin challenge resulted in increased Fn protein levels in the lungs from WT mice compared to controls, whereas Tnc (either variant) and Postn levels were not altered (Figure 3G). The levels of all of these proteins were significantly reduced in bleomycin-challenged *Fbln1c*$^{-/-}$ mice compared to WT controls. Tnc and Postn levels were significantly reduced even compared with non-bleomycin treated controls. We also measured the deposition of other ECM components, versican and ECM1, but found no significant differences between bleomcyin-challenged WT and *Fbln1c*$^{-/-}$ mice compared to controls (not shown).

Fbln1c binds with latent TGF-β binding protein-1 (LTBP1) to activate TGF-β. To investigate the mechanisms involved in Fbln1c-regulated pulmonary fibrosis, we measured the levels of TGF-β, its activation and regulation in the lungs of bleomycin-challenged mice. The mRNA levels of *Tgfb* were increased in the lung tissues of bleomycin-challenged WT and *Fbln1c*$^{-/-}$ mice (Figure 4A). The levels of active TGF-β1 proteins measured by ELISA were increased in WT, however, levels of active TGF-β1 did not increase in *Fbln1c*$^{-/-}$ mice (Figure 4B). LTBP1 protein regulates TGF-β1

activation, and its levels were increased in both WT and *Fbln1c*$^{-/-}$ mice after bleomycin challenge, with no significant differences between them (Figure 4C). We then measured the downstream molecules in the TGF-β signaling pathway, Smad2, Smad3, and Smad4. Bleomycin challenge significantly reduced *Smad3* mRNA levels (Supplementary Figure 5A) but increased phosphorylated Smad3 (pSmad3) protein levels in the lungs of WT but not *Fbln1c*$^{-/-}$ mice (Figure 4D). In contrast, the mRNA levels of *Smad2* and *Smad4* in lungs of WT and *Fbln1c*$^{-/-}$ mice were not altered (Supplementary Figure 5, B and C).

To further assess mechanisms, we immunoprecipitated Fbln1c and identified its binding relationship with LTBP1. LTBP1 proteins were detectable when immunoprecipitated with Fbln1c from naïve WT mouse lung lysates assessed using immunoblot (Figure 4E). This did not occur in proteins from *Fbln1c*$^{-/-}$ mice. This confirmed that a binding interaction exists between Fbln1c and LTBP1.

Collectively these data show that the absence of Fbln1c does not affect LTBP1 levels but that Fbln1c is required for the activation of TGF-β1 and downstream Smad3 phosphorylation.

Fbln1c regulates fibroblast activation, conversion into myofibroblasts and collagen deposition. To further investigate the role of Fbln1c in the mechanisms of pathogenesis of fibrosis, primary lung fibroblasts were isolated from WT and *Fbln1c*$^{-/-}$ mice, and stimulated with recombinant TGF-β1 protein. As we stimulated fibroblasts with recombinant TGF-β1 protein, we could not distinguish between TGF-β1 protein that was administered versus that secreted. Thus, we measured *Tgfb* mRNA levels. *Tgfb* mRNA (Figure 5A) and LTBP1 protein (Figure 5B) levels were increased in lung fibroblasts from both WT and *Fbln1c*$^{-/-}$ mice after stimulation. Thus, the levels of TGF-

β1 message and LTBP1 were again unchanged in fibroblasts. Downstream pSmad3 protein levels were also increased in WT but again not *Fbln1c*$^{-/-}$ fibroblasts after stimulation (Figure 5C).

TGF-β-stimulated fibroblasts from WT mice developed into myofibroblasts, as indicated by the presence of α-smooth muscle actin (SMA), but this was significantly reduced in *Fbln1c*$^{-/-}$ mice (Figure 5D). TGF-β-stimulated fibroblasts from WT mice had significantly increased Col1a1 mRNA (Figure 5E) and protein (Figure 5F) levels, but these were reduced and completely inhibited, respectively, in *Fbln1c*$^{-/-}$ fibroblasts.

To further explore the role of Fbln1c in the TGF-β signalling pathway, we isolated primary fibroblasts from WT mouse lungs and treated them with bronchoalveolar lavage fluid (BALF, 20μl per mouse from 6 mice pooled to a total of 120μl) from WT or *Fbln1c*$^{-/-}$ mice 28 days after bleomycin challenge or controls, for 24 and 48 hours. However, fibroblasts from *Fbln1c*$^{-/-}$ but not WT mice were detached and dead at these time points. We therefore isolated fibroblasts at an earlier time point (6 hours) and lysates were collected. Smad2, 3 and 4 gene expression were largely unaltered in fibroblasts cultured with BALF from WT and *Fbln1c*$^{-/-}$ mice (Supplementary Figure, 5D–F). Col1a1 protein levels were also not changed in fibroblasts incubated with BALF from bleomycin-challenged compared to control WT mice. However, Col1a1 and pSmad3 proteins were reduced in cells treated with BALF from Fbln1c$^{-/-}$ compared to WT mice (Figure 5G and H).

Fbln1 colocalized with LTBP1 in lungs from IPF patients. We show that Fbln1c binds to LTBP1 (Figure 4E) to regulate TGF-β activation (Figure 4B) in mouse lungs. To further confirm this binding relationship in humans, we stained lung sections from IPF patients and controls with Fbln1 and LTBP1, and assessed their colocalization. We

detected Fbln1 here due to lack of a specific antibody to distinguish human Fbln1c by immunofluorescence. Fbln1 and LTBP1 protein colocalized in lung sections from IPF patients but not non-IPF controls (Figure 6).

Discussion

Aberrant deposition of ECM proteins and fibrosis has severe pathological consequences in many diseases including in the respiratory tract, but no effective treatments currently exist. Here we identify a critical role for the ECM protein, Fbln1c, in regulating airway and lung remodeling during the pathogenesis of pulmonary fibrosis. For the first time we showed specific increases in Fbln1c protein levels in the lungs of IPF patients. Increased collagen and Fbln1c deposition were also observed around the airways and in the lung tissues in experimental bleomycin-induced pulmonary fibrosis. Genetic inhibition of *Fbln1c* prevented increases in bleomycin-induced collagen around the airways and in lungs, inhibited MMP expression and also protected against the impairment of lung function. Fbln1c also bound to Fn and Tnc and these ECM proteins and Postn were reduced with genetic inhibition. We discovered a novel pro-fibrotic mechanism whereby Fbln1c bound to LTBP1 to induce TGF-β activation the downstream Smad3 pathway and collagen deposition, as well as the conversion of fibroblasts to myofibroblasts (Figure 7). We validated these experimental links by showing that Fbln1c colocalized with LTBP1 in the lung tissues of IPF patients.

Several experimental models are available to examine lung fibrosis, all of which have limitations. We employed the widely used bleomycin-induced mouse model of pulmonary fibrosis to show that Fbln1c is increased around the airways and lungs. The concern with this model is that the bleomycin-induced fibrosis is partially reversible,

unlike human lung fibrosis (26). However, it does develop similar histological alterations to those observed in IPF patients, and the use of this model and analysis of transgenic mice have greatly advanced our understanding of the disease (26).

Through its interaction with multiple ECM proteins, Fbln1c was revealed to play a major role in directing ECM deposition in pulmonary fibrosis. *Fbln1c*$^{-/-}$ mice were completely protected against collagen deposition around the small airways and in whole lung tissues. Type I collagen is the most abundant ECM protein in the lung that constitutes the majority of the matrix structure. Collagen production can be regulated by fibroblast activation, inflammation, alterations in the balance of enzymes that cleave and promote fiber assembly, crosslinking and stability of the ECM. Fbln1 is known to bind many other ECM proteins to stabilize the structure (27).

MMPs, particularly MMP1, 8, and 13, are prevalent proteases that degrade ECM proteins in the lung. MMP1 (protein) and MMP3 (protein and mRNA) levels are increased in the lungs of IPF patients, and *Mmp3*$^{-/-}$ mice are protected against bleomcyin-induced lung fibrosis (28). MMP8 protein levels are also increased in the BALF from IPF patients and in the lungs of mice with bleomcyin-induced pulmonary fibrosis (29). We also found that MMPs were significantly increased in WT mouse lungs after bleomycin challenge. MMP activity is counterbalanced by the inhibitory activity of TIMPs (30), accordingly we showed *Timp1* mRNA expression was also increased in WT mouse lungs after bleomcyin challenge. Notably the aberrant levels of *Mmps* and *Timp1* were not observed in *Fbln1c*$^{-/-}$ mice, identifying a potential role for Fbln1c in regulating MMP/TIMP activity in pulmonary fibrosis. MMPs are known to be able to limit the extent of fibrosis and may be induced to control remodeling. Thus, in the absence of Fibln1c and fibrosis MMP responses are not needed. It remains unknown

how Fbln1c regulates MMPs and TIMPs, and if the effects are direct or indirect, which requires further study.

Few studies have examined alterations in lung function in the bleomycin model, but we demonstrated the impairment of tissue damping, tissue elastance and compliance, that are relevant to IPF physiology (31). Tissue damping is a measure of whole lung tissue resistance, while tissue elastance and compliance indicate the level of lung stiffness (32). Our lung function results demonstrate that the lungs of bleomycin-challenged WT mice stiffen due to fibrosis, as occurs in IPF patients (33, 34). However, these lung function changes do not develop in the absence of *Fbln1c*, indicating its critical role in pulmonary fibrosis. Deletion of total *Fbln1* in mice results in perinatal lethality, but *Fbln1c*$^{-/-}$ mice develop a normal phenotype (1). Thus, therapeutically targeting Fbln1c, rather than total Fbln1, may potentially limit adverse effects resulting from the total disruption of Fbln1's role in tissue homeostasis.

Other ECM proteins are also involved in the pathogenesis of IPF. Lung fibroblasts from IPF patients secrete more Fn and have the capacity to increase Tnc synthesis compared to those from healthy controls (35). We showed that Fn and Tnc deposition increased around small airways after bleomycin challenge of WT mice, and that Fbln1c was necessary for these increases. Furthermore, Fn, Tnc and Postn protein levels in whole lung tissues were reduced in bleomycin-challenged *Fbln1c*$^{-/-}$ mice compared to WT controls. The ECM proteins, Fn and Tnc were selected because of their known interactions with Fbln1 (1), while Postn was chosen for its indirect binding to Fbln1 and its effects on collagen deposition (36). It is likely that other ECM proteins are involved in the regulation of matrix deposition. For example, versican affects the early stage of repair processes in IPF (37), however its protein levels were not changed in lungs between WT and *Fbln1c*$^{-/-}$ mice (data not shown). The protein

levels of elastin are increased in fibrotic lung tissue in IPF patients (38), and many other ECM proteins may also be involved (39). However, a complete characterization of the complex interactions that contribute to the generation of aberrant ECM is beyond the scope of a single study. Levels of ECM proteins may also be affected by changes in other factors that control their transcription such as microRNAs, which have also been shown to be dysregulated in IPF(2), and other chronic fibrosis associated diseases (40).

TGF-β is the archetypal pro-fibrotic cytokine, that is increased in IPF lungs (18) and promotes cell proliferation and remodeling processes. It is initially synthesized in a precursor form, dimerizes and is cleaved by the protease furin (41). This results in the release of a small latent complex which attaches to LTBP1 (41). Anchoring of this complex to the ECM occurs through interactions of ECM proteins with the epidermal growth factor (EGF)-like repeats domains on N-terminus of the LTBP1 protein (42). From the anchored complex activated TGF-β is released via several mechanisms which induce downstream signaling pathways (43). Fbln1c contains EGF-like binding regions (16), which in itself indicates a potential role in TGF-β activation. We showed that Fbln1 and LTBP1 colocalized in lungs from IPF patients. Interestingly, monkey Fbln1c was reported to interact with heparin-binding EGF-like modules (44). Other studies show that Fbln5 binds to the N-terminal EGF-like domain of LTBP2 (45). We showed that Fbln1c binds with LTBP1 and regulates TGF-β activation. TGF-β signaling *via* Smad effectors is well known to be involved in cell growth and proliferation, and ECM deposition in fibroblasts (43). Previous studies demonstrated reduced Smad3 mRNA and protein levels in the lungs of mice with bleomycin-induced pulmonary fibrosis (46). We corroborated these decreases in *Smad3* mRNA expression but in contrast found increased pSmad3 protein levels in WT mouse lungs after bleomycin

challenge and fibroblasts after TGF-β stimulation. However, the altered pSmad3 levels did not occur in the absence of *Fbln1c*. This demonstrates roles for Fbln1c in controling TGF-β activation and signaling pathways that lead to pulmonary fibrosis.

We found that lung fibroblasts from WT mice incubated with BALF from *Fbln1c*$^{-/-}$ mice for 6 hours reduce pSamd3 and collagen proteins compared to those cells received BALF from WT mice. Longer incubations (24 and 48 hours) with BALF from *Fbln1c*$^{-/-}$ mice result in fibroblasts detached from plates. The exact reason remains unclear, while the fibroblasts detachment may be due to decreased collagen. Many studies have shown that collagen is essential to assist fibroblasts attachment (47). LTBP1 is secreted into the airway fluid, however, the lack of active TGF-β in the BALF of Fbln1c$^{-/-}$ mice reduced the collagen levels in fibroblasts. This further supports our findings that Fbln1c regulates TGF-β activation.

Integrins are cell membrane receptors that facilitate ECM protein binding and adhesion. They are also involved in TGF-β activation, Sheppard et al., showed that inhibition of the expression of the αv subunit reduced TGF-β levels in fibroblasts and protected against fibrosis in an experimental animal model of liver fibrosis (47, 48). This study also suggested that αvβ1 integrin is a major regulator of TGF-β activation. There are several therapeutic compounds that target the αv integrin that are currently in clinical trials to reduce fibrosis (48). Previous studies showed that Fbln1c might be mediated through αvβ1 integrin signalling, however, the relationship between Fbln1c and integrins in lung fibrosis remains unknown.

ECM proteins are deposited in excess in many pulmonary diseases, and Fbln1, in particular Fbln1c is involved in regulating remodeling and fibrosis in lungs (1, 20). We have shown that genetic inhibition of Fbln1c in mice substantially reduced pulmonary remodeling and fibrosis in cigarette smoke-induced COPD and house duct

mite-induced asthma (1, 20). Our previous studies also showed that specific inhibition of Fbln1c gene expression with siRNA also similarly reduced remodeling features. Thus, targeting the Fbln1c gene, for example with antisense oligonucleotides, may be a therapeutic option to reduce fibrosis in lungs. We show that Fbln1c regulates fibrosis by binding with LTBP1 to control TGF-β activation. Inhibiting Fbln1c binding to LTBP1 binding is another potential therapeutic option to reduce active TGF-β and lung fibrosis.

We showed that TGF-β-induced conversion of fibroblasts to myofibroblasts is substantially reduced in the absence of Fbln1c. Fibroblasts/myofibroblasts are the major cellular source of collagen (49). These cells have altered autophagic pathways in IPF patients (50), produce more Fbln1 (18) and are important in maintaining a pathologic pro-fibrotic phenotype, particularly in a collagen rich environment (51).

We previously showed that Fbln1, but not specifically Fbln1c, protein levels were increased in the serum/plasma and lung tissue of IPF patients (18). Fbln1, like other ECM proteins, is constantly being produced and degraded. This is partly due to the activity of specific proteases, such as MMP13 (52). Peptide products resulting from ECM degradation are not necessarily inert, and may have immunomodulatory effects. Peptides from ECM degradation induce the proliferation, migration and MMP production and ECM deposition of airway smooth muscle (ASM) cells and myofibroblasts (53, 54). Protein fragments generated by MMP activity are increased in the serum of IPF patients compared to healthy controls, and are associated with disease progression (55). Other studies showed that Fbln1c peptides increase the attachment of ASM cells and fibroblasts (19). Also, Fbln1c peptide stimulates Fbln1 deposition in fibroblasts from lPF patients, and augments the production of Fn and perlecan (19). Thus, the increase in Fbln1 and Fbln1c may provide substrates for

MMPs to generate peptide fragments that contribute to the development of remodeling and disease in IPF.

Considering previous and our new data together, Fbln1c associates with Fn, Tnc and Postn to stabilize the resulting collagen structure. It also induces increased MMP activity that drives the production of ECM fragments further stimulating fibroblast activity and perpetuating fibrosis. Collectively these events promote the deposition and stabilize exaggerated ECM formation around the airways and in lung tissues in IPF. We propose (Figure 7) that excess Fbln1c is induced during remodeling events and promotes the development of fibrosis. TGF-β precursors dimerize and are cleaved by the endopeptidase furin to form small latent complexes (41). LTBP1 binds to these complexes and the entire combination is secreted into the extracellular space (42). Fbln1c protein binds to LTBP1 *via* EGF-like domains causing the release of activated TGF-β. It also regulates fibroblasts activation, the TGF-β signaling pathway to induce myofibroblast development and collagen production. This provides our fundamental knowledge of fibrosis and further increases understanding of mechanism of TGF-β activation. Thus, Fbln1c may be a novel therapeutic target for suppressing fibrosis in IPF and potentially other fibrotic diseases.

Methods

Human lung tissue. Lung tissue for Fbln1c immunohostochemistry staining (Figure 1A) was obtained from patients with IPF (n=7). All IPF patients had end stage diseases and underwent lung transplantation (Table 1). The non-IPF control group (n=8) consisted of 4 donor lungs that were not used in transplantation, and lung tissues from 4 sujects with normal lung function (FEV1 > 80% and FEV1:FVC ratio > 0.7) who had lung tissue removed for thoracic malignancies. Human tissues for co-localization

immunohistochemical staining (Figure 6) were procured from non-transplantable donors and IPF patients undergoing lung transplantation or lung resection.

Immunohistochemistry and remodeling. Human and mouse lung longitudinal sections on slides were incubated with citrate buffer (10 mM sodium citrate, 0.05% Tween 20, pH 6) for antigen retrieval after deparaffinization. Lung sections were blocked with casein (Sigma-Aldrich, USA) at room temperature (RT) for 1 h. Slides were incubated with monoclonal anti-Fbln1c antibody (mAB5D12, 1:50), which was produced as previously described (16), and Fbln1 (1:50, Abcam, UK), Col1a1 (1:100, Abcam), Tnc (1:50, Santa Cruz Biotechnology, USA), Fn (1:100, Sigma-Aldrich, USA), and Postn (1: 100, Abcam) antibodies, at 4°C overnight, followed by anti-rabbit secondary antibody (R&D systems, USA) at RT for 1 h. Diaminobenzidine (DAB, DAKO, Australia) was applied and hematoxylin was used to counterstain the sections. Lung remodeling analyses were assessed as previously described (1, 18).

Mice and experimental model. Six to eight-week-old female WT C57BL/6J or *Fbln1c*$^{-/-}$ mice were house in specific pathogen-free conditions. *Fbln1c*$^{-/-}$ mice were generated as previously described (1). Experimental pulmonary fibrosis was induced by administration of a single dose of bleomycin sulfate (0.05 U/mouse, MP Biomedical, USA) as described previously (21-23). Controls received an equal volume of sterile PBS. Tissues were collected 7, 14, 21 and 28 days after bleomycin challenge.

Lung remodeling. Formalin-fixed, paraffin embedded mouse lung sections were deparaffinized with xylene and a graded ethanol series (56). Collagen was stained with Verhoff's-Van Gieson stain (Australian Biostain, Australia). Fbln1, Fbln1c, Fn, Tnc and

Postn were stained by immunofluorescence or immunohistochemistry. Photomicrographs were taken with an Axio Imager M2 microscope (Zeiss, Germany) and images evaluated with image J (version 1.47, NIH, USA) as previously described (23, 57, 58). Briefly, at least 6 airways per mouse were blind-selected from 4–8 animals in each group and images captured with an Aperio AT2 (Leica Biosystems, Germany). Mouse small airways were defined as those having the perimeter of the basement membrane (Pbm) less than 1 mm (59). The Pbm, the inner collagen area (Ai) and the outer collagen area (Ao) were manually measured using Image J. The collagen area (Wct) was calculated (Wct=Ao-Ai) and normalized to the Pbm. For quantification in whole lungs, Fbln1c area was normalized to total area as previously described (18).

Hydroxyproline. Hydroxyproline content in mouse whole lung tissues were assessed as a measure of lung collagen levels. Content was measured colorimetrically as previously described (1, 60, 61).

Soluble collagen assay. Soluble collagen was determined using Sircol Collagen Assay kits (S1000, Biocolor, UK) according to the manufacturer's instructions with modifications as previously described (1).

Protein extraction and immunoblotting. Mouse lung tissues were snap frozen and thawed before being homogenized in radioimmunoprecipitation assay (RIPA) buffer (Sigma-Aldrich, Australia) supplemented with PhosSTOP phosphatase inhibitor and complete protease inhibitor cocktails (Roche, Germany) and centrifuged (8,000x*g*, 10min, 4°C) as previously described(58, 62). Proteins were collected for immunoblot

or ELISA assays. Protein concentrations were determined using a BCA protein assay kit (Pierce Biotechnology, USA).

Proteins were separated by SDS-PAGE electrophoresis using Mini-PROTEAN TGX Stain-Free gels (Bio-Rad, USA), and transferred to polyvinylidene fluoride membranes (EMD Millipore, USA)(63). Proteins of interest were detected proteins of interest were detected using Fbln1 (1:2000, ab175204, Abcam), the Fbln1c antibody described above, Col1a1 (1:5000, ab34170, Abcam), Tnc (1:500, sc20932, Santa Cruz Biotechnology), Fn (1:4000, F3648, Sigma-Aldrich), Postn (1:4000, ab14041, Abcam), LTBP1 (1:1000, abs504, EMD Millipore, USA), phosphorylated Smad3 (1:2000, ab52903, Abcam), vinculin (1:10,000, ab129002, Abcam), and β-actin (1:10,000, ab8227, Abcam) antibodies at 4°C overnight. Blots were incubated with anti-mouse (ab97023, Abcam) or anti-rabbit horseradish peroxidase-conjugated secondary antibody (HAF008, R&D systems) at RT for 2 h. Images of immunoblots were captured with a ChemiDoc MP System (Bio-Rad, USA). Some blots were cut based on the protein molecular weight. Image J was used for densitometry analysis as described previously (1, 64).

Immunofluorescence. Mouse and human lungs were formalin-fixed, and paraffin embedded (1, 56, 65, 66). Sections were cut to 4 μm thickness. Slides were deparaffinized and incubated with Tris buffer (10 mM Tris base, 0.5% Tween 20, pH 9) at 100°C for antigen retrieval, and blocked with casein (Sigma-Aldrich) at RT for 2 h. Slides were stained with the Fbln1c antibody (1:20) that were conjugated with FITC using a kit (ab102884, Abcam) at 4°C overnight. Nuclei were counterstained with Hoechst (1:200, Sigma-Aldrich) at RT for 5 min (65). Images were taken using Axio Imager M2 microscope.

Mouse primary fibroblasts were fixed with 3% paraformadelyde in PBS (pH 7.4) at RT for 10 min, permeabilized with 0.2% Triton X-100, blocked with casein at RT for 1 h, and incubated with anti-mouse β-actin antibody (1:1000, ab8227, Abcam) at RT for 1 h. After three PBS-T washes, cells were incubated with FITC conjugated anti-mouse secondary antibody (1:1000, ab6717, Abcam) at RT for 1 h. Cells were incubated with a Cy3 conjugated anti-mouse α-SMA antibody (1:200, c6198, Sigma-Aldrich) at RT for 2 h, and nuclei were counterstained with Hoechst. Ten random images per section were visualized using an Axio Imager M2 microscope (Zeiss, Germany) and analyzed using imaging software (Zen, Zeiss). The percentage of myofibroblasts was calculated as the percentage of α-SMA positive cells in the total cell number (β-actin positive cells).

Human lung sections were deparaffinized, incubated with citrate for antigen retrieval at 100°C for 15 min. Slides were incubated overnight with anti-Fbln1 (1:50, ab211536, Abcam) in PBS+1%BSA at 4°C overnight, followed by anti-mouse Alexa647 conjugated secondary antibody (1:100, A-31571, ThermoFisher Scientific, Netherland) at RT for 2 h. After washing the slides with PBS, they were incubated with anti-LTBP1 (1:100, ab78294, Abcam) at RT for 2 h, followed by anti-rabbit Alexa555 conjugated secondary antibody (1: 100, A-31572 ThermoFisher Scientific). Nuclei were counterstained with DAPI (10236276001, Sigma-Aldrich). Fluorescence signals were examined using a Leica TCS SP8 confocal microscope (Leica Microsystems, Germany).

ELISA. Cytokines in lung tissues were assessed by ELISA as previously described (58, 67). The concentrations of TGF-β were determined using capture and detection antibodies (555052 and 555053, BD Pharmingen, Australia), according to the

manufacturer's instructions. The levels of target proteins in lungs were normalized to total lung protein.

Immunoprecipitation. Fbln1c proteins were immunoprecipitated from lung homogenates from WT and *Fbln1c*$^{-/-}$ mice using a Dynabead protein A immunoprecipitation kit (10006D, Life Technologies, USA) according to the manufacturer's instructions. Briefly, Fbln1c antibody (10 μg) was added to lung homogenates and incubated with rotation at 4°C overnight. Dynabeads (1.5 mg), superparamagnetic particles that have specific affinity to bind to antibody, were added into protein and antibody complex and incubated with rotation at 4°C for 1 h. The bead–antibody and protein complex were separated from the solution by magnet. Non-binding proteins were washed off three times with PBS and target proteins were collected by adding elution buffer (from kit) and Laemmli sample buffer (1610747, Bio-Rad) containing 2-mercaptoethanol (1610710, Bio-Rad), and heated at 90°C for 10 mins. SDS-PAGE was used to detect the target Fbln1c protein and its binding partners.

RNA extraction and quantitative real-time PCR (qRT-PCR). Total RNA was extracted using TRIzol (Invitrogen, USA), and reverse transcribed using Bioscript (Bioline, USA), and random hexamer primers (Invitrogen). qRT-PCR was performed using SYBR reagents and a Viia 7 real-time PCR system (Life Technologies). Primers are listed in Table 2. mRNA levels were normalized to those of the housekeeping gene hypoxanthine-guanine phosphoribosyltransferase (HPRT), and expressed as relative abundance to the control group (67, 68).

SHG microscopy. Formalin fixed paraffin embedded mouse lung sections were cut to 10 μm thickness. Sections were deparaffinized with xylene and a graded ethanol series, then dehydrated and coverslipped for SHG using a Leica SP5 multiphoton confocal system with an excitation wavelength of 810 nm throughout. SHG forward (F_{SHG}) and backward (B_{SHG}) signals were obtained and image analysis was performed using Fiji with images imported from LAS AF software as previously described (24, 69). In brief, a quarter wave plate (CVI Laser Optics, Albuquerque, USA) was used to produce circularly polarized light to detect maximum collagen content. The incident laser power was adjusted to the same level (25 mW) throughout the experiment, and SHG signals were detected with a 405/10-nm band pass filter. Ten random pictures without large airways and blood vessels were selected. The pixel area (the number of pixels with intensity above threshold) and total signal intensity (total intensity for all pixels with intensity above threshold) was determined, and the average values calculated for every image in the stack. The process was repeated for both F_{SHG} and B_{SHG} propagated signals. The ratio of F_{SHG}/B_{SHG} signal was then calculated for area measurements.

Lung function. Mice were anesthetized (50 μL/10g, intraperitoneally) with a mix of xylazine (2 mg/ml, Troy laboratories, Australia) and ketamine (40 mg/ml, Parnell, Australia). Mice were tracheotomized and a cannula was inserted into the trachea. Animals were ventilated with a tidal volume of 8 mL/kg at a rate of 450 breaths/min, with increased airway pressure from 2 to 30 cmH_2O into mouse lungs to measure baseline lung function parameters, including tissue damping, tissue elastance and lung compliance using invasive plethysmography with the forced oscillation technique and Flexivent apparatus (Scireq, Canada) as previously described (1, 56, 58, 70).

570

571 *Lung fibroblast isolation and culture.* Lungs were excised from six-week old WT or
572 *Fbln1c*$^{-/-}$ mice, and primary fibroblasts were isolated as described previously (71, 72).
573 The cells were cultured in Dulbecco's modified eagle's medium (DMEM, D5671,
574 Sigma-Aldrich) containing 10% fetal bovine serum (FBS, Bovogen, Australia), 25 mmol
575 hydroxyethylpiperazine-N'-2-ethanesulfonic acid (HEPES) buffer, 100 U/mL penicillin,
576 and 100 µg/mL streptomycin (37°C, 5% CO_2), and used from passage 3–7. Primary
577 fibroblasts were seeded at 5,000 cells/cm^2 and incubated overnight to allow cells to
578 form a monolayer. Fibroblasts were stimulated with recombinant TGF-β protein (5
579 ng/mL, R&D system) supplemented with 0.5% FCS in DMEM or media only (control)
580 for 48 h. Cell lysates were collected for RNA and protein extraction, and myofibroblasts
581 were analyzed using immunofluorescence.

582 Lung fibroblasts were isolated from WT mice and cultured in 6-well plates with
583 BALF (20µl each mouse, 6 mice per group, 120µl in total in 1 ml DMEM media with
584 10% FCS) from bleomycin-challenged or control WT and Fbln1c$^{-/-}$ mice for 6, 24 and
585 48 hours. Cell lysates were collected for protein analysis.

586

587 *Statistics.* Results are presented as mean ± standard error of the mean (SEM) from 7-
588 8 human samples or 6–8 mice in duplicate or triplicate experiments. Statistical
589 significance of data between two groups was determined using a two-tailed student t-
590 test, and more than two groups were analyzed using one-way analysis of variance
591 (ANOVA) with Bonferroni post-test and Prism-GraphPad Software (version 6,
592 GraphPad, USA). Statistical differences were accepted at $P<0.05$.

593

Study approvals. All procedures were approved by The University of Newcastle or the University Medical Centre Groningen Human and Animal Ethics Committees.

Author Contributions

G.L, A.G.J, J.C.H, J.K.B, and P.M.H, participated in the design of the study. G.L performed *in vivo* and part of the *in vitro* experiments. M.A.C and W.S.A generated *Fbln1c*$^{-/-}$ mice and provided Fbln1c antibody. P.M.N, T.J.H, C.L.H and B.J assisted with mouse experiments. A.C.H and M.F assisted with immunoprecipitation experiments. G.T performed SHG experiments. B.G.O and J.K.B performed human lung collections. T.B performed human colocalization experiment. D.A.K assisted with experimental design. N.G.H contributed to preparation and editing of manuscript. All authors participated in the interpretation of data, preparation and editing of manuscript for intellectual content. All authors read and approved the final manuscript (with the exception of W.S.A who passed away before the final version was completed).

Acknowledgements

This work was supported as follows. G.L was supported by Lung Foundation Australia/Lizotte Family Research Award. The NIH to W.S.A, and M.C.C. A.G.J was supported by Lung Foundation of Australia/Boehringer Ingelheim COPD research Fellowship. B.G.O and J.K.B were supported by NHMRC Career Development Fellowships. J.K.B was supported by a University of Groningen/European Union Rosalind Franklin Fellowship. Fellowships and grants from National Health and Medical Research Council (NHMRC) of Australia (NHMRC #1079187) and the Brawn Foundation, Faculty of Health and Medicine, The University of Newcastle to P.M.H. This work is dedicated to the memory of Professor W. Scott Argraves who passed

away during the completion of this study. The authors declare no competing financial interests.

References

1. Liu G, Cooley MA, Jarnicki AG, Hsu ACY, Nair PM, Haw TJ, et al. Fibulin-1 regulates the pathogenesis of tissue remodeling in respiratory diseases. *JCI Insight.* 2016;1(9): e36380.
2. Ge L, Habiel DM, Hansbro PM, Kim RY, Gharib SA, Edelman JD, et al. miR-323a-3p regulates lung fibrosis by targeting multiple profibrotic pathways. *JCI Insight.* 2016;1(20):e90301.
3. Wynn TA. Integrating mechanisms of pulmonary fibrosis. *J Exp Med.* 2011;208(7):1339-50.
4. Adachi K, Yamauchi K, Bernaudin JF, Fouret P, Ferrans VJ, and Crystal RG. Evaluation of fibronectin gene expression by in situ hybridization. Differential expression of the fibronectin gene among populations of human alveolar macrophages. *Am J Pathol.* 1988;133(2):193-203.
5. Uchida M, Shiraishi H, Ohta S, Arima K, Taniguchi K, Suzuki S, et al. Periostin, a matricellular protein, plays a role in the induction of chemokines in pulmonary fibrosis. *Am J Respir Cell Mol Biol.* 2012;46(5):677-86.
6. King TE, Jr., Bradford WZ, Castro-Bernardini S, Fagan EA, Glaspole I, Glassberg MK, et al. A phase 3 trial of pirfenidone in patients with idiopathic pulmonary fibrosis. *N Engl J Med.* 2014;370(22):2083-92.
7. Navaratnam V, Fleming KM, West J, Smith CJ, Jenkins RG, Fogarty A, et al. The rising incidence of idiopathic pulmonary fibrosis in the U.K. *Thorax.* 2011;66(6):462-7.
8. Raghu G, Collard HR, Egan JJ, Martinez FJ, Behr J, Brown KK, et al. An official ATS/ERS/JRS/ALAT statement: idiopathic pulmonary fibrosis: evidence-based guidelines for diagnosis and management. *Am J Respir Crit Care Med.* 2011;183(6):788-824.
9. King TE, Jr., Pardo A, and Selman M. Idiopathic pulmonary fibrosis. *Lancet.* 2011;378(9807):1949-61.
10. Ponticos M, Holmes AM, Shi-wen X, Leoni P, Khan K, Rajkumar VS, et al. Pivotal role of connective tissue growth factor in lung fibrosis: MAPK-dependent transcriptional activation of type I collagen. *Arthritis Rheum.* 2009;60(7):2142-55.
11. Crouch E. Pathobiology of pulmonary fibrosis. *Am J Physiol.* 1990;259(4 Pt 1):L159-84.
12. Collard HR, King TE, Jr., Bartelson BB, Vourlekis JS, Schwarz MI, and Brown KK. Changes in clinical and physiologic variables predict survival in idiopathic pulmonary fibrosis. *Am J Respir Crit Care Med.* 2003;168(5):538-42.
13. Lawson WE, Grant SW, Ambrosini V, Womble KE, Dawson EP, Lane KB, et al. Genetic mutations in surfactant protein C are a rare cause of sporadic cases of IPF. *Thorax.* 2004;59(11):977-80.
14. Pardo A, and Selman M. Lung Fibroblasts, Aging, and Idiopathic Pulmonary Fibrosis. *Annals of the American Thoracic Society.* 2016;13(Supplement_5):S417-s21.
15. Richeldi L, du Bois RM, Raghu G, Azuma A, Brown KK, Costabel U, et al. Efficacy and safety of nintedanib in idiopathic pulmonary fibrosis. *N Engl J Med.* 2014;370(22):2071-82.
16. Argraves WS, Tran H, Burgess WH, and Dickerson K. Fibulin is an extracellular matrix and plasma glycoprotein with repeated domain structure. *J Cell Biol.* 1990;111(6 Pt 2):3155-64.

17. Roark EF, Keene DR, Haudenschild CC, Godyna S, Little CD, and Argraves WS. The association of human fibulin-1 with elastic fibers: an immunohistological, ultrastructural, and RNA study. *J Histochem Cytochem.* 1995;43(4):401-11.
18. Jaffar J, Unger S, Corte TJ, Keller M, Wolters PJ, Richeldi L, et al. Fibulin-1 predicts disease progression in patients with idiopathic pulmonary fibrosis. *Chest.* 2014;146(4):1055-63.
19. Ge Q, Chen L, Jaffar J, Argraves WS, Twal WO, Hansbro P, et al. Fibulin1C peptide induces cell attachment and extracellular matrix deposition in lung fibroblasts. *Sci Rep.* 2015;5:9496.
20. Liu G, Cooley MA, Nair PM, Donovan C, Hsu AC, Jarnicki AG, et al. Airway remodelling and inflammation in asthma are dependent on the extracellular matrix protein fibulin-1c. *J Pathol.* 2017;243(4):510-23.
21. Hattori N, Degen JL, Sisson TH, Liu H, Moore BB, Pandrangi RG, et al. Bleomycin-induced pulmonary fibrosis in fibrinogen-null mice. *J Clin Invest.* 2000;106(11):1341-50.
22. Xiao J, Meng XM, Huang XR, Chung AC, Feng YL, Hui DS, et al. miR-29 inhibits bleomycin-induced pulmonary fibrosis in mice. *Mol Ther.* 2012;20(6):1251-60.
23. Gold MJ, Hiebert PR, Park HY, Stefanowicz D, Le A, Starkey MR, et al. Mucosal production of uric acid by airway epithelial cells contributes to particulate matter-induced allergic sensitization. *Mucosal Immunol.* 2016;9(3):809-20.
24. Tjin G, Xu P, Kable SH, Kable EP, and Burgess JK. Quantification of collagen I in airway tissues using second harmonic generation. *J Biomed Opt.* 2014;19(3):36005.
25. Tjin G, White ES, Faiz A, Sicard D, Tschumperlin DJ, Mahar A, et al. Lysyl oxidases regulate fibrillar collagen remodelling in idiopathic pulmonary fibrosis. *Dis Model Mech.* 2017;10(11):1301-12.
26. Moore BB, and Hogaboam CM. Murine models of pulmonary fibrosis. *Am J Physiol Lung Cell Mol Physiol.* 2008;294(2):L152-60.
27. de Vega S, Iwamoto T, and Yamada Y. Fibulins: multiple roles in matrix structures and tissue functions. *Cell Mol Life Sci.* 2009;66(11-12):1890-902.
28. Yamashita CM, Dolgonos L, Zemans RL, Young SK, Robertson J, Briones N, et al. Matrix metalloproteinase 3 is a mediator of pulmonary fibrosis. *Am J Pathol.* 2011;179(4):1733-45.
29. Craig VJ, Polverino F, Laucho-Contreras ME, Shi Y, Liu Y, Osorio JC, et al. Mononuclear phagocytes and airway epithelial cells: novel sources of matrix metalloproteinase-8 (MMP-8) in patients with idiopathic pulmonary fibrosis. *PLoS One.* 2014;9(5):e97485.
30. Dancer RC, Wood AM, and Thickett DR. Metalloproteinases in idiopathic pulmonary fibrosis. *Eur Respir J.* 2011;38(6):1461-7.
31. Vanoirbeek JA, Rinaldi M, De Vooght V, Haenen S, Bobic S, Gayan-Ramirez G, et al. Noninvasive and invasive pulmonary function in mouse models of obstructive and restrictive respiratory diseases. *Am J Respir Cell Mol Biol.* 2010;42(1):96-104.
32. Fritz DK, Kerr C, Fattouh R, Llop-Guevara A, Khan WI, Jordana M, et al. A mouse model of airway disease: oncostatin M-induced pulmonary eosinophilia, goblet cell hyperplasia, and airway hyperresponsiveness are STAT6 dependent, and interstitial pulmonary fibrosis is STAT6 independent. *J Immunol.* 2011;186(2):1107-18.

719 33. Booth AJ, Hadley R, Cornett AM, Dreffs AA, Matthes SA, Tsui JL, et al. Acellular
720 normal and fibrotic human lung matrices as a culture system for in vitro
721 investigation. *Am J Respir Crit Care Med.* 2012;186(9):866-76.
722 34. Clarke DL, Carruthers AM, Mustelin T, and Murray LA. Matrix regulation of
723 idiopathic pulmonary fibrosis: the role of enzymes. *Fibrogenesis Tissue Repair.*
724 2013;6(1):20.
725 35. Estany S, Vicens-Zygmunt V, Llatjos R, Montes A, Penin R, Escobar I, et al.
726 Lung fibrotic tenascin-C upregulation is associated with other extracellular
727 matrix proteins and induced by TGFbeta1. *BMC Pulm Med.* 2014;14:120.
728 36. Norris RA, Damon B, Mironov V, Kasyanov V, Ramamurthi A, Moreno-
729 Rodriguez R, et al. Periostin regulates collagen fibrillogenesis and the
730 biomechanical properties of connective tissues. *J Cell Biochem.*
731 2007;101(3):695-711.
732 37. Bensadoun ES, Burke AK, Hogg JC, and Roberts CR. Proteoglycan deposition
733 in pulmonary fibrosis. *Am J Respir Crit Care Med.* 1996;154(6 Pt 1):1819-28.
734 38. Blaauboer ME, Boeijen FR, Emson CL, Turner SM, Zandieh-Doulabi B,
735 Hanemaaijer R, et al. Extracellular matrix proteins: a positive feedback loop in
736 lung fibrosis? *Matrix Biol.* 2014;34:170-8.
737 39. Burgess JK, Boustany S, Moir LM, Weckmann M, Lau JY, Grafton K, et al.
738 Reduction of tumstatin in asthmatic airways contributes to angiogenesis,
739 inflammation, and hyperresponsiveness. *Am J Respir Crit Care Med.*
740 2010;181(2):106-15.
741 40. Conickx G, Mestdagh P, Avila Cobos F, Verhamme FM, Maes T,
742 Vanaudenaerde BM, et al. MicroRNA Profiling Reveals a Role for MicroRNA-
743 218-5p in the Pathogenesis of Chronic Obstructive Pulmonary Disease. *Am J*
744 *Respir Crit Care Med.* 2017;195(1):43-56.
745 41. Fortunel NO, Hatzfeld A, and Hatzfeld JA. Transforming growth factor-beta:
746 pleiotropic role in the regulation of hematopoiesis. *Blood.* 2000;96(6):2022-36.
747 42. Kanzaki T, Olofsson A, Moren A, Wernstedt C, Hellman U, Miyazono K, et al.
748 TGF-beta 1 binding protein: a component of the large latent complex of TGF-
749 beta 1 with multiple repeat sequences. *Cell.* 1990;61(6):1051-61.
750 43. ten Dijke P, and Arthur HM. Extracellular control of TGFbeta signalling in
751 vascular development and disease. *Nat Rev Mol Cell Biol.* 2007;8(11):857-69.
752 44. Brooke JS, Cha JH, and Eidels L. Latent transforming growth factor beta-
753 binding protein-3 and fibulin-1C interact with the extracellular domain of the
754 heparin-binding EGF-like growth factor precursor. *BMC Cell Biol.* 2002;3:2.
755 45. Hirai M, Horiguchi M, Ohbayashi T, Kita T, Chien KR, and Nakamura T. Latent
756 TGF-beta-binding protein 2 binds to DANCE/fibulin-5 and regulates elastic fiber
757 assembly. *The EMBO journal.* 2007;26(14):3283-95.
758 46. Zhao Y, and Geverd DA. Regulation of Smad3 expression in bleomycin-induced
759 pulmonary fibrosis: a negative feedback loop of TGF-beta signaling. *Biochem*
760 *Biophys Res Commun.* 2002;294(2):319-23.
761 47. Jokinen J, Dadu E, Nykvist P, Kapyla J, White DJ, Ivaska J, et al. Integrin-
762 mediated cell adhesion to type I collagen fibrils. *J Biol Chem.*
763 2004;279(30):31956-63.
764 48. Henderson NC, Arnold TD, Katamura Y, Giacomini MM, Rodriguez JD, McCarty
765 JH, et al. Targeting of alphav integrin identifies a core molecular pathway that
766 regulates fibrosis in several organs. *Nat Med.* 2013;19(12):1617-24.
767 49. Phan SH. The myofibroblast in pulmonary fibrosis. *Chest.* 2002;122(6
768 Suppl):286S-9S.

50. Ricci A, Cherubini E, Scozzi D, Pietrangeli V, Tabbi L, Raffa S, et al. Decreased expression of autophagic beclin 1 protein in idiopathic pulmonary fibrosis fibroblasts. *J Cell Physiol.* 2013;228(7):1516-24.
51. Nho RS, and Hergert P. IPF fibroblasts are desensitized to type I collagen matrix-induced cell death by suppressing low autophagy via aberrant Akt/mTOR kinases. *PLoS One.* 2014;9(4):e94616.
52. Wang Q, Shen B, Chen L, Zheng P, Feng H, Hao Q, et al. Extracellular calumenin suppresses ERK1/2 signaling and cell migration by protecting fibulin-1 from MMP-13-mediated proteolysis. *Oncogene.* 2015;34(8):1006-18.
53. Lopez B, Gonzalez A, and Diez J. Role of matrix metalloproteinases in hypertension-associated cardiac fibrosis. *Curr Opin Nephrol Hypertens.* 2004;13(2):197-204.
54. Harkness LM, Weckmann M, Kopp M, Becker T, Ashton AW, and Burgess JK. Tumstatin regulates the angiogenic and inflammatory potential of airway smooth muscle extracellular matrix. *J Cell Mol Med.* 2017;21(12):3288-97.
55. Jenkins RG, Simpson JK, Saini G, Bentley JH, Russell AM, Braybrooke R, et al. Longitudinal change in collagen degradation biomarkers in idiopathic pulmonary fibrosis: an analysis from the prospective, multicentre PROFILE study. *Lancet Respir Med.* 2015;3(6):462-72.
56. Thorburn AN, Foster PS, Gibson PG, and Hansbro PM. Components of Streptococcus pneumoniae suppress allergic airways disease and NKT cells by inducing regulatory T cells. *J Immunol.* 2012;188(9):4611-20.
57. Hansbro PM, Hamilton MJ, Fricker M, Gellatly SL, Jarnicki AG, Zheng D, et al. Importance of mast cell Prss31/transmembrane tryptase/tryptase-gamma in lung function and experimental chronic obstructive pulmonary disease and colitis. *J Biol Chem.* 2014;289(26):18214-27.
58. Haw TJ, Starkey MR, Nair PM, Pavlidis S, Liu G, Nguyen DH, et al. A pathogenic role for tumor necrosis factor-related apoptosis-inducing ligand in chronic obstructive pulmonary disease. *Mucosal Immunol.* 2016;9(4):859-72.
59. Palmans E, Kips JC, and Pauwels RA. Prolonged allergen exposure induces structural airway changes in sensitized rats. *Am J Respir Crit Care Med.* 2000;161(2 Pt 1):627-35.
60. Woessner JF, Jr. The determination of hydroxyproline in tissue and protein samples containing small proportions of this imino acid. *Arch Biochem Biophys.* 1961;93:440-7.
61. Jarnicki AG, Schilter H, Liu G, Wheeldon K, Essilfie AT, Foot JS, et al. The inhibitor of semicarbazide-sensitive amine oxidase, PXS-4728A, ameliorates key features of chronic obstructive pulmonary disease in a mouse model. *Br J Pharmacol.* 2016;173(22):3161-75.
62. Kim RY, Horvat JC, Pinkerton JW, Starkey MR, Essilfie AT, Mayall JR, et al. MicroRNA-21 drives severe, steroid-insensitive experimental asthma by amplifying phosphoinositide 3-kinase-mediated suppression of histone deacetylase 2. *J Allergy Clin Immunol.* 2016.
63. Kim RY, Pinkerton JW, Essilfie AT, Robertson AAB, Baines KJ, Brown AC, et al. Role for NLRP3 Inflammasome-mediated, IL-1beta-Dependent Responses in Severe, Steroid-Resistant Asthma. *Am J Respir Crit Care Med.* 2017;196(3):283-97.
64. Hsu AC, Starkey MR, Hanish I, Parsons K, Haw TJ, Howland LJ, et al. Targeting PI3K-p110alpha Suppresses Influenza Virus Infection in Chronic Obstructive Pulmonary Disease. *Am J Respir Crit Care Med.* 2015;191(9):1012-23.

65. Kaiko GE, Phipps S, Hickey DK, Lam CE, Hansbro PM, Foster PS, et al. Chlamydia muridarum infection subverts dendritic cell function to promote Th2 immunity and airways hyperreactivity. *J Immunol.* 2008;180(4):2225-32.
66. Liu G, Mateer SW, Hsu A, Goggins BJ, Tay H, Mathe A, et al. Platelet activating factor receptor regulates colitis-induced pulmonary inflammation through the NLRP3 inflammasome. *Mucosal Immunol.* 2019;12(4):862-73.
67. Essilfie AT, Horvat JC, Kim RY, Mayall JR, Pinkerton JW, Beckett EL, et al. Macrolide therapy suppresses key features of experimental steroid-sensitive and steroid-insensitive asthma. *Thorax.* 2015;70(5):458-67.
68. Asquith KL, Horvat JC, Kaiko GE, Carey AJ, Beagley KW, Hansbro PM, et al. Interleukin-13 promotes susceptibility to chlamydial infection of the respiratory and genital tracts. *PLoS Pathog.* 2011;7(5):e1001339.
69. Kottmann RM, Sharp J, Owens K, Salzman P, Xiao GQ, Phipps RP, et al. Second harmonic generation microscopy reveals altered collagen microstructure in usual interstitial pneumonia versus healthy lung. *Respir Res.* 2015;16:61.
70. Preston JA, Essilfie AT, Horvat JC, Wade MA, Beagley KW, Gibson PG, et al. Inhibition of allergic airways disease by immunomodulatory therapy with whole killed Streptococcus pneumoniae. *Vaccine.* 2007;25(48):8154-62.
71. Hinz B, Celetta G, Tomasek JJ, Gabbiani G, and Chaponnier C. Alpha-smooth muscle actin expression upregulates fibroblast contractile activity. *Mol Biol Cell.* 2001;12(9):2730-41.
72. Seluanov A, Vaidya A, and Gorbunova V. Establishing primary adult fibroblast cultures from rodents. *J Vis Exp.* 2010(44).

844 **Table 1. Human subject history**
845

Donor	Gender	Age	Diagnosis	Smoking history
Non-IPF control 1	Male	30	Resection for thoracic malignancy	None
Non-IPF control 2	Female	62	Resection for thoracic malignancy	Ex-smoker
Non-IPF control 3	Male	47	MVA	None
Non-IPF control 4	Male	60	Emphysema	Ex-smoker
Non-IPF control 5	Female	62	Resection for thoracic malignancy	Ex-smoker
Non-IPF control 6	Male	19	MVA	None
Non-IPF control 7	Male	52	Healthy-haemorrhage	None
Non-IPF control 8	Female	62	Emphysema	None
IPF 1	Female		IPF	None
IPF 2	Male	52	IPF	None
IPF 3	Male	57	IPF	Ex-smoker
IPF 4	Male	55	IPF	Ex-smoker
IPF 5	Female	58	IPF	None
IPF 6	Male	58	IPF	Ex-smoker
IPF 7	Male	58	IPF	None

846
847 MVA: Motor vehicle accident
848 All IPF patients were end stage and had lung transplantation

849 **Table 2. Primers for qRT-PCR**

Gene	Forward primer 5' to 3'	Reverse primer 5' to 3'
Col1a1	CTTCACCTACAGCACCCTTGTG	TGACTGTCTTGCCCCAAGTTC
Fbln1c	AGAACTATCGCCGCTCCGCA	CCACCGCTGGCACTTGGATG
Fbln1d	GCTATGAGGACGGCATGACT	GGAAACTACGCCTCCCAACA
Fn	TGTGGTTGCCTTGCACGAT	GCTATCCACTGGGCAGTAAAGC
HPRT	AGGCCAGACTTTGTTGGATTTGAA	CAACTTGCGCTCATCTTAGGCTTT
MMP1	GTCTTCTGGCACACGCTTTT	GGGCAGCAACAATAAACAA
MMP3	ACATGGAGACTTTGTCCCTTTTG	TTGGCTGAGTGGTAGAGTCCC
MMP8	GATTCAGAAGAAACGTGGACTCAA	CATCAAGGCACCAGGATCAGT
MMP12	GCTTGAGTTTTGATGGTGTCAC	GAAGTAATGTTGGTGGCTGGGA
MMP13	CCTTCTGGTCTTCTGGCACAC	GGCTGGGTCACACTTCTCTGG
Postn	CACGGCATGGTTATTCCTTCA	TCAGGACACGGTCAATGACAT
Smad2	AATACGGTAGATCAGTGGGACA	CAGTTTTCGATTGCCTTGAGC
Smad3	GTTCTCCAAACCTCTCCCCG	TGTGAGGCGTGGAATGTCTC
Smad4	AGCCGTCCTTACCCACTGAA	GGTGGTAGTGCTGTTATGATGGT
TGF-β	CCCGAAGCGGACTACTATGCTA	GGTAACGCCAGGAATTGTTGCTAT
TIMP1	ATCTGGCATCCTCTTGTTGCT	CTCGTTGATTTCTGGGGAACC
Tnc	TCCCCAAGAGAATTTACAGCTACAG	AGATTCATAGACCAGGAGGTATCCA

850

851 **Figure legends**

852 **Figure 1. Fbln1c is increased in IPF patients and bleomycin-induced**
853 **experimental pulmonary fibrosis.** (**A**) Fbln1c deposition in lung sections from non-
854 fibrotic are and fibrotic area in IPF patients and lung healthy controls were stained
855 using immunohistochemistry (left), scale bar = 200 μm; Fbln1c-stained areas were
856 quantified with normalization to the total area (right, n=7–8). A single bleomycin
857 challenge was used to induce pulmonary fibrosis in WT and *Fbln1c*$^{-/-}$ mice. Controls
858 were challenged with PBS. (**B**) Stained areas of total Fbln1 were quantified around
859 small airways with normalization to the Pbm (n=6-8). (**C**) Fbln1 protein levels were
860 assessed using immunoblot of whole lung tissues (left), and fold change of
861 densitometry normalized to β-actin and quantified (right, n=8). (**D**) Twenty-eight days
862 after bleomycin or PBS challenge, lung sections were assessed for protein of the 1c
863 isoform, Fbln1c, around small airways using immunofluorescence (left), scale bar=50
864 μm, (inserts show expanded images of indicated regions; scale bar=15 μm);
865 quantification of Fbln1c-stained areas around airways was quantified with
866 normalization to the Pbm (right, n=8). (**E**) Fbln1c protein area in parenchyma was
867 determined using immunofluorescence (left), scale bar=50 μm; Fbln1c-stained areas
868 were quantified with normalization to total area (right, n=8). (**F**) Fbln1c protein levels
869 were assessed in whole lungs using immunoblot (top), and fold change of densitometry
870 quantified with normalization to β-actin (bottom, n=8). Statistical differences were
871 determined with two-tailed student t-test. *P<0.05, **P<0.01, ***P<0.001, ****P<0.0001
872 compared to human healthy lung controls or PBS-challenged mouse controls.
873

874 **Figure 2. Bleomycin challenge of *Fbln1c*$^{-/-}$ mice does not induce airway or lung**
875 **fibrosis or impair lung function.** A single bleomycin challenge was used to induce

pulmonary fibrosis in WT and *Fbln1c*$^{-/-}$ mice that were assessed 28 days later. Controls received PBS. (**A**) *Fbln1c* and (**B**) *Fbln1d* mRNA levels in whole lungs determined using qRT-PCR (n=6-8). (**C**) Lung sections were stained with Verheoff's-Van Gieson stain (left, scale bar=500 μm; inserts show expanded images of indicated regions; scale bar=50 μm), and areas of collagen around small airways quantified with normalization to the perimeter of basement membrane (right, n=8). (**D**) Total collagen levels were assessed by measuring hydroxyproline (left), and soluble collagen (right) in the whole lung tissues (n=8). (**E**) Type I collagen (*Col1a1*) mRNA levels were measured in whole lungs using qRT-PCR (n=8). (**F**) Col1a1 protein levels were measured in whole lungs using immunoblot (left), and fold change quantified with normalization to β-actin (right, n=8). (**G**) Collagen fibers were detected by second harmonic generation (SHG) microscopy (left), and fiber areas were calculated by forwards (F_{SHG})/backwards (B_{SHG}) SHG ratios (right, n=4–6, scale bar=100 μm). Lung function in terms of (**H**) tissue damping, tissue elastance (**I**), and lung compliance (**J**) were measured using invasive plethysmography and the forced oscillation technique (n=5-8). Statistical differences were determined with one-way ANOVA followed by Bonferroni post-test. *P<0.05, **P<0.01, ****P<0.0001 compared to PBS-challenged WT or *Fbln1c*$^{-/-}$ controls. †P<0.05, ††P<0.01 compared to bleomycin-challenged WT controls. NS=not significant.

Figure 3. Bleomycin challenge in *Fbln1c*$^{-/-}$ mice does not increase the levels of ECM proteins around the small airway or in whole lung tissue. A single bleomycin challenge was used to induce pulmonary fibrosis in WT and *Fbln1c*$^{-/-}$ mice that were assessed 28 days later. Controls received PBS. (**A**) Fibronectin (Fn), (**B**) tenascin-c (Tnc) and (**C**) periostin (Postn) deposition in the basement membrane around small

901 airways was assessed using immunohistochemistry, and stained areas quantified with
902 normalization to the perimeter of basement membrane (n=24-40 airways from n=4-8
903 mice per group). *Fn* (**D**), *Tnc* (**E**) and *Postn* (**F**) mRNA levels in lungs were determined
904 using qRT-PCR (n=6-8). (**G**) Fn, Tnc (variant 1 and 2) and Postn protein levels in whole
905 lung tissues were assessed using immunoblot (top), and fold change quantified using
906 densitometry with normalization to β-actin (bottom, n=5-8). Statistical differences were
907 determined with one-way ANOVA followed by Bonferroni post-test. *P<0.05, **P<0.01
908 compared to PBS-challenged WT controls. †P<0.05, ††P<0.01, ††††P<0.0001 compared
909 to bleomycin-challenged WT controls.
910
911 **Figure 4. Fbln1c binds with LTBP1 to induce TGF-β activation.** A single bleomycin
912 challenge was used to induce pulmonary fibrosis in WT and *Fbln1c*$^{-/-}$ mice that were
913 assessed 28 days later. Controls received PBS. TGF-β (**A**) mRNA and (**B**) active
914 protein levels in whole lung tissues measured using qRT-PCR and ELISA (n=4-8). (**C**)
915 LTBP1 protein levels in lungs measured using immunoblot (left), and fold change
916 quantification using densitometry with normalization to β-actin (right, n=5-8). (**D**)
917 Phosphorylated Smad3 protein levels in lungs measured using immunoblot (left), and
918 fold change quantified using densitometry with normalization to vinculin (right, n=5-8).
919 (**E**) Immunoprecipitation (IP) of Fbln1c protein from whole lung tissues, and detection
920 of Fbln1c and LTBP1 binding using immunoblot (IB). Immunoblot analysis of lung
921 tissues before (input) and after IP. Statistical differences were determined with one-
922 way ANOVA followed by Bonferroni post-test. *P<0.05, **P<0.01 compared to PBS-
923 challenged WT controls. †P<0.05 compared to bleomycin-challenged WT controls.
924

Figure 5. Fbln1c binds to LTBP1 to activate TGF-β and induce fibroblast activation and collagen deposition. A single bleomycin challenge was used to induce pulmonary fibrosis in WT and *Fbln1c*$^{-/-}$ mice that were assessed 28 days later. Controls received PBS. (**A**) *Tgf-β* mRNA levels in lungs were measured using qRT-PCR (n=6). (**B**) LTBP1 protein levels in whole lung tissues were measured using immunoblot (left), and fold change quantified using densitometry with normalization to β-actin (right, n=6). Primary lung fibroblasts were isolated from whole lung tissues of naïve WT and *Fbln1c*$^{-/-}$ mice and stimulated with TGF-β or media control. (**C**) Phosphorylated *Smad3* protein levels in fibroblast lysates were measured using immunoblot (left), and fold change quantified using densitometry with normalization to vinculin (right, n=6). (**D**) Fibroblasts were stained with β-actin, and myofibroblasts were stained with α-SMA (left), and the percentage of myofibroblasts as a percentage of total fibroblasts determined (right, bar=500 μm, n=6). (**E**) *Col1a1* mRNA levels in fibroblast lysates were measured using qRT-PCR (n=6). (**F**) Col1a1 protein levels in fibroblast lysates were measured using immunoblot, and fold change quantified using densitometry with normalization to β-actin (right, n=6). Primary mouse lung fibroblasts from WT mice were incubated with bronchoalveolar lavage fluid (BALF, 20μl each mouse, 120μl total) from WT and *Fbln1c*$^{-/-}$ mice after 28 days bleomycin challenge and controls for 6 hours. (**G**) Col1a1 and pSamd3 protein in fibroblast lysates were measured using immunoblot, and (**H**) fold change quantified using densitometry with normalization to vinculin (right, n=6). Statistical differences were determined with one-way ANOVA followed by Bonferroni post-test. *P<0.05, **P<0.01, ***P<0.001, ****P<0.0001 compared to WT fibroblasts controls. †P<0.05, ††P<0.01 compared to TGF-β-stimulated WT fibroblasts controls.

Figure 6. Fbln1 and LTBP1 colocalizes in IPF patient lungs. Lung sections were obtained from IPF patients and controls. Fbln1 (red) and LTBP1 (green) were stained using immunofluorescence, and nuclei were stained with DAPI (blue). Scale bar=50 μm.

Figure 7. Proposed role of Fbln1c in pulmonary fibrosis: Fbln1c binds to latent TGF-β binding protein-1 (LTBP1) to activate TGF-β, and induce myofibroblast proliferation and collagen production. TGF-β precursors dimerize and are cleaved by the endopeptidase furin to form small latent complexes. Latent TGF-β binding protein 1 (LTBP1) binds to small latent complexes and the entire combination is secreted into the extracellular space. Fbln1c protein binds to LTBP1 likely *via* EGF-like domains on both causing the release of activated TGF-β. Fbln1c-induced activated TGF-β binds to its receptor on the surface of fibroblasts to stimulate the development and proliferation of myofibroblasts through the activity of phosphorylated Smad3 causing increased collagen production and pulmonary fibrosis. Fbln1c also associates with Fn, Tnc and Postn to stabilize the resulting collagen structure.

Figures and figure legends

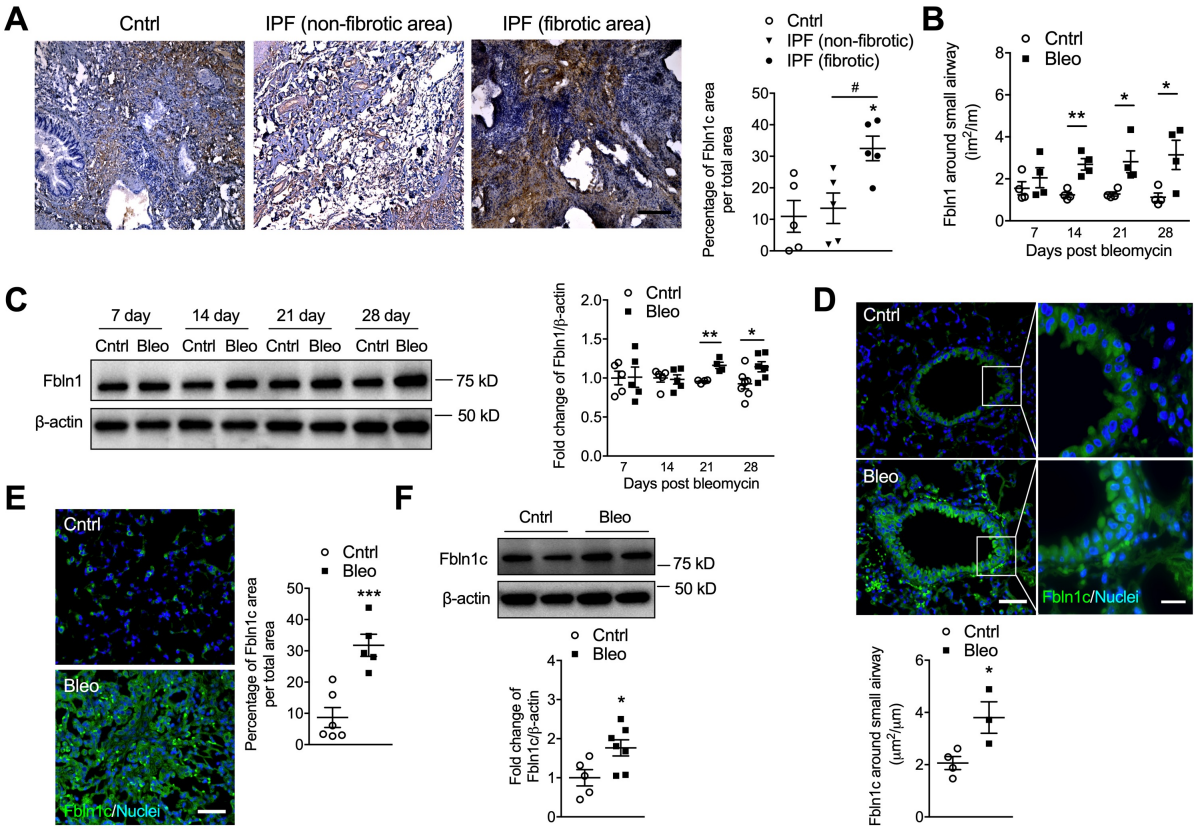

Figure 1. Fbln1c is increased in IPF patients and bleomycin-induced experimental pulmonary fibrosis. (**A**) Fbln1c deposition in lung sections from non-fibrotic are and fibrotic area in IPF patients and lung healthy controls were stained using immunohistochemistry (left), scale bar = 200 μm; Fbln1c-stained areas were quantified with normalization to the total area (right, n=7–8). A single bleomycin challenge was used to induce pulmonary fibrosis in WT and *Fbln1c*$^{-/-}$ mice. Controls were challenged with PBS. (**B**) Stained areas of total Fbln1 were quantified around small airways with normalization to the Pbm (n=6-8). (**C**) Fbln1 protein levels were assessed using immunoblot of whole lung tissues (left), and fold change of densitometry normalized to β-actin and quantified (right, n=8). (**D**) Twenty-eight days after bleomycin or PBS challenge, lung sections were assessed for protein of the 1c isoform, Fbln1c, around small airways using immunofluorescence (left), scale bar=50 μm, (inserts show expanded images of indicated regions; scale bar=15 μm); quantification of Fbln1c-stained areas around airways was quantified with normalization to the Pbm (right, n=8). (**E**) Fbln1c protein area in parenchyma was determined using immunofluorescence (left), scale bar=50 μm; Fbln1c-stained areas were quantified with normalization to total area (right, n=8). (**F**) Fbln1c protein levels were assessed in whole lungs using immunoblot (top), and fold change of densitometry quantified with normalization to β-actin (bottom, n=8). Statistical differences were determined with two-tailed student t-test. *P<0.05, **P<0.01, ***P<0.001, ****P<0.0001 compared to human healthy lung controls or PBS-challenged mouse controls.

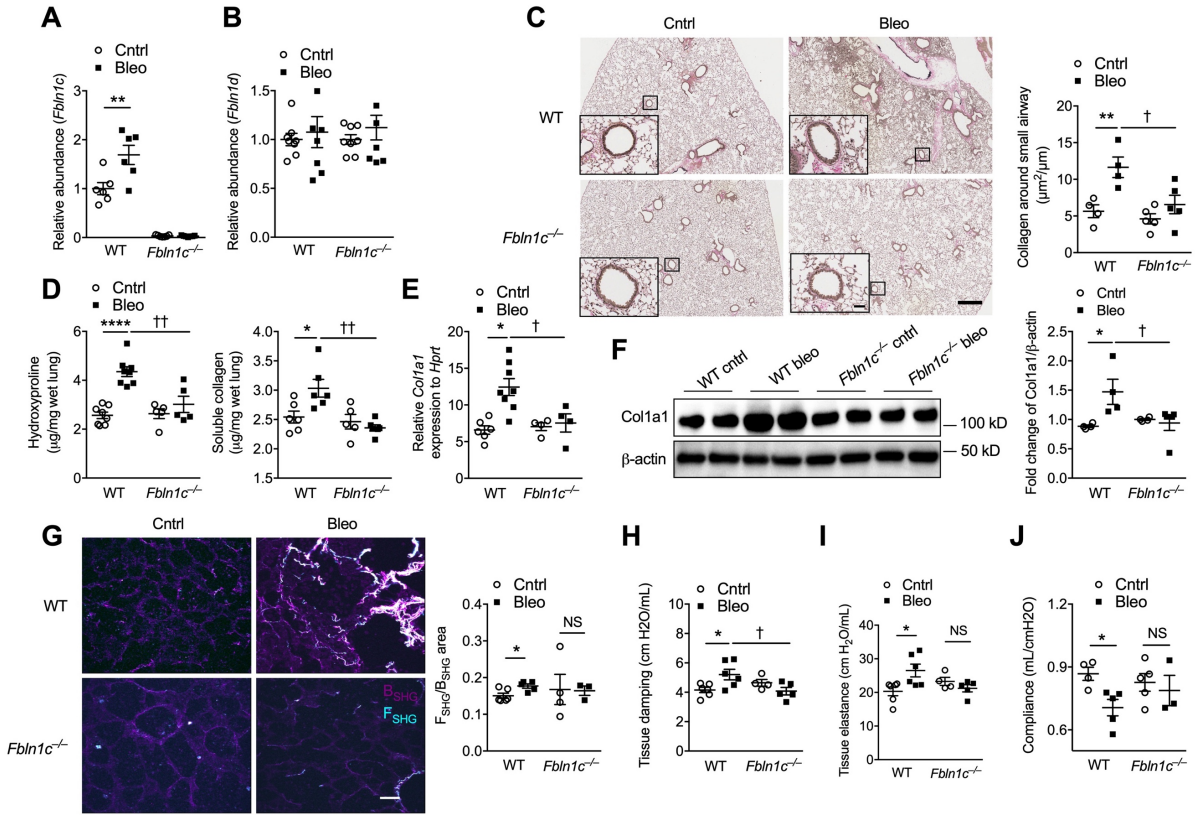

Figure 2. Bleomycin challenge of *Fbln1c*$^{-/-}$ mice does not induce airway or lung fibrosis or impair lung function. A single bleomycin challenge was used to induce pulmonary fibrosis in WT and *Fbln1c*$^{-/-}$ mice that were assessed 28 days later. Controls received PBS. (**A**) *Fbln1c* and (**B**) *Fbln1d* mRNA levels in whole lungs determined using qRT-PCR (n=6-8). (**C**) Lung sections were stained with Verheoff's-Van Gieson stain (left, scale bar=500 μm; inserts show expanded images of indicated regions; scale bar=50 μm), and areas of collagen around small airways quantified with normalization to the perimeter of basement membrane (right, n=8). (**D**) Total collagen levels were assessed by measuring hydroxyproline (left), and soluble collagen (right) in the whole lung tissues (n=8). (**E**) Type I collagen (*Col1a1*) mRNA levels were measured in whole lungs using qRT-PCR (n=8). (**F**) Col1a1 protein levels were measured in whole lungs using immunoblot (left), and fold change quantified with normalization to β-actin (right, n=8). (**G**) Collagen fibers were detected by second harmonic generation (SHG) microscopy (left), and fiber areas were calculated by forwards (F_{SHG})/backwards (B_{SHG}) SHG ratios (right, n=4–6, scale bar=100 μm). Lung function in terms of (**H**) tissue damping, tissue elastance (**I**), and lung compliance (**J**) were measured using invasive plethysmography and the forced oscillation technique (n=5-8). Statistical differences were determined with one-way ANOVA followed by Bonferroni post-test. *P<0.05, **P<0.01, ****P<0.0001 compared to PBS-challenged WT or *Fbln1c*$^{-/-}$ controls. †P<0.05, ††P<0.01 compared to bleomycin-challenged WT controls. NS=not significant.

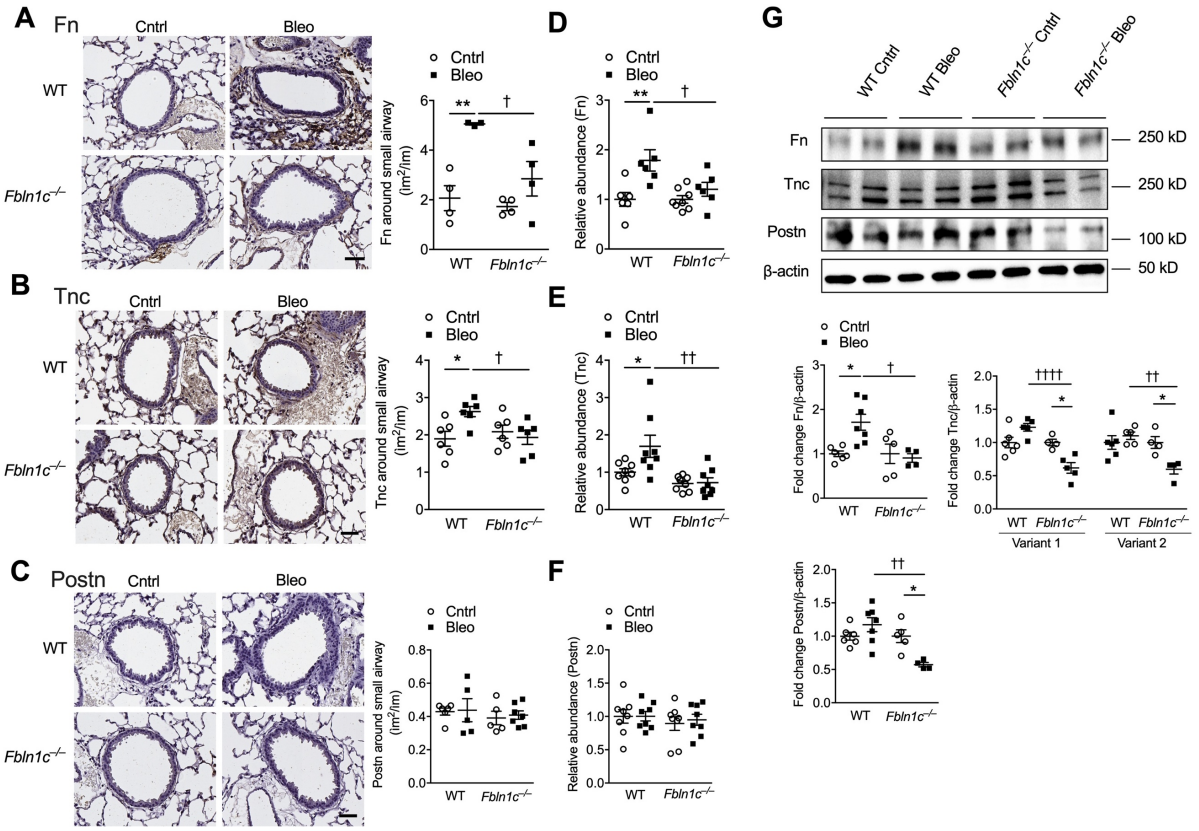

Figure 3. Bleomycin challenge in *Fbln1c*$^{-/-}$ mice does not increase the levels of ECM proteins around the small airway or in whole lung tissue. A single bleomycin challenge was used to induce pulmonary fibrosis in WT and *Fbln1c*$^{-/-}$ mice that were assessed 28 days later. Controls received PBS. (**A**) Fibronectin (Fn), (**B**) tenascin-c (Tnc) and (**C**) periostin (Postn) deposition in the basement membrane around small airways was assessed using immunohistochemistry, and stained areas quantified with normalization to the perimeter of basement membrane (n=24-40 airways from n=4-8 mice per group). *Fn* (**D**), *Tnc* (**E**) and *Postn* (**F**) mRNA levels in lungs were determined using qRT-PCR (n=6-8). (**G**) Fn, Tnc (variant 1 and 2) and Postn protein levels in whole lung tissues were assessed using immunoblot (top), and fold change quantified using densitometry with normalization to β-actin (bottom, n=5-8). Statistical differences were determined with one-way ANOVA followed by Bonferroni post-test. *P<0.05, **P<0.01 compared to PBS-challenged WT controls. †P<0.05, ††P<0.01, ††††P<0.0001 compared to bleomycin-challenged WT controls.

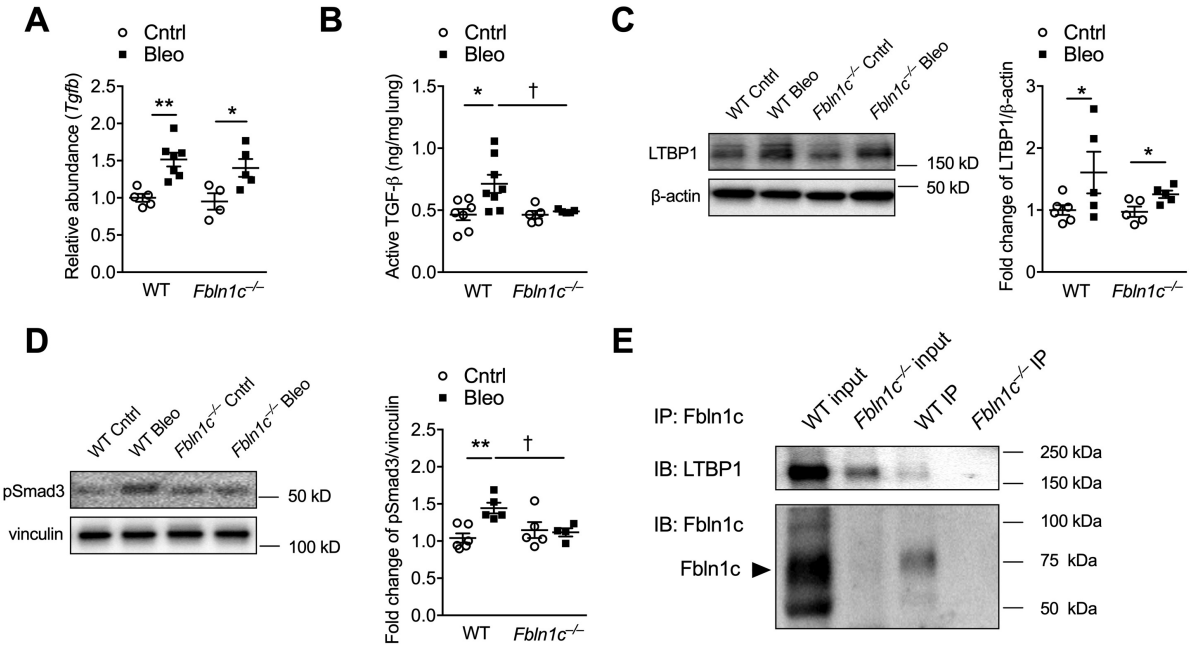

Figure 4. Fbln1c binds with LTBP1 to induce TGF-β activation. A single bleomycin challenge was used to induce pulmonary fibrosis in WT and *Fbln1c*$^{-/-}$ mice that were assessed 28 days later. Controls received PBS. TGF-β (**A**) mRNA and (**B**) active protein levels in whole lung tissues measured using qRT-PCR and ELISA (n=4-8). (**C**) LTBP1 protein levels in lungs measured using immunoblot (left), and fold change quantification using densitometry with normalization to β-actin (right, n=5-8). (**D**) Phosphorylated Smad3 protein levels in lungs measured using immunoblot (left), and fold change quantified using densitometry with normalization to vinculin (right, n=5-8). (**E**) Immunoprecipitation (IP) of Fbln1c protein from whole lung tissues, and detection of Fbln1c and LTBP1 binding using immunoblot (IB). Immunoblot analysis of lung tissues before (input) and after IP. Statistical differences were determined with one-way ANOVA followed by Bonferroni post-test. *P<0.05, **P<0.01 compared to PBS-challenged WT controls. †P<0.05 compared to bleomycin-challenged WT controls.

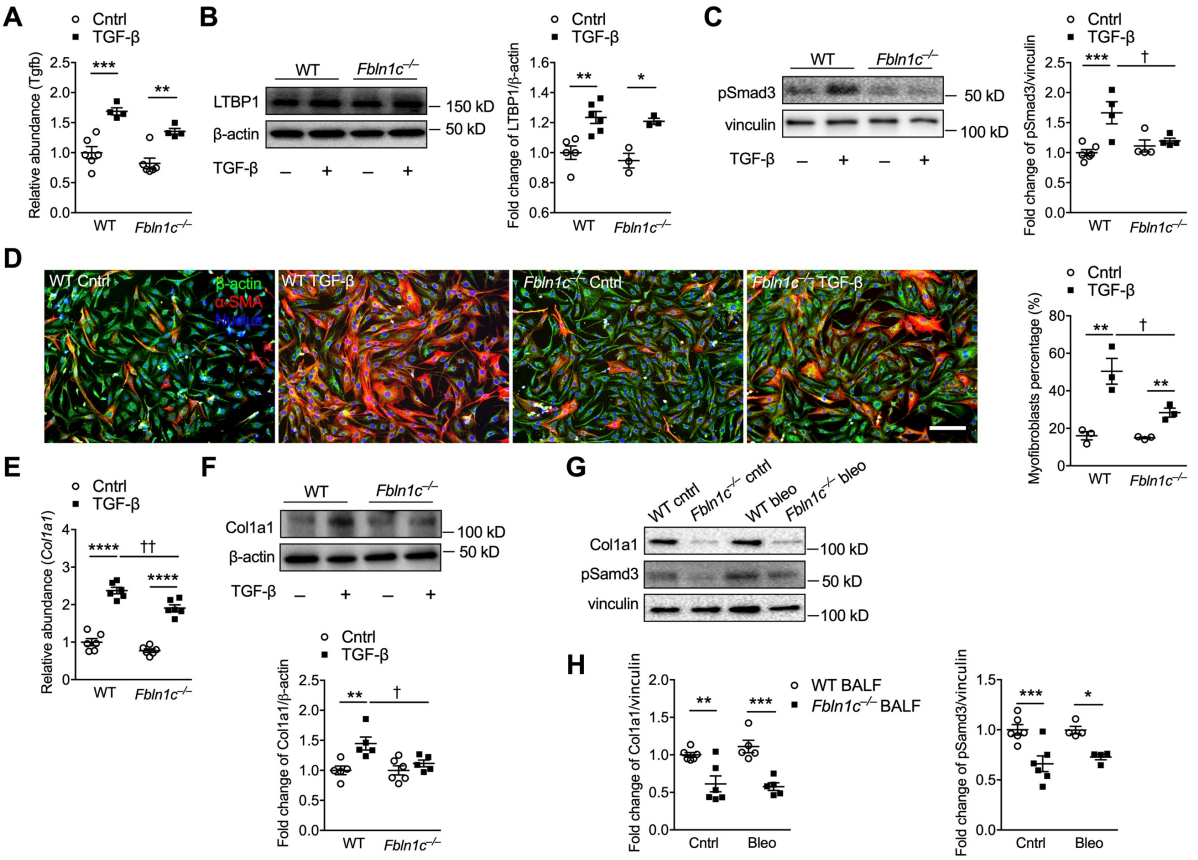

Figure 5. Fbln1c binds to LTBP1 to activate TGF-β and induce fibroblast activation and collagen deposition. A single bleomycin challenge was used to induce pulmonary fibrosis in WT and *Fbln1c*$^{-/-}$ mice that were assessed 28 days later. Controls received PBS. (**A**) *Tgf-β* mRNA levels in lungs were measured using qRT-PCR (n=6). (**B**) LTBP1 protein levels in whole lung tissues were measured using immunoblot (left), and fold change quantified using densitometry with normalization to β-actin (right, n=6). Primary lung fibroblasts were isolated from whole lung tissues of naïve WT and *Fbln1c*$^{-/-}$ mice and stimulated with TGF-β or media control. (**C**) Phosphorylated *Smad3* protein levels in fibroblast lysates were measured using immunoblot (left), and fold change quantified using densitometry with normalization to vinculin (right, n=6). (**D**) Fibroblasts were stained with β-actin, and myofibroblasts were stained with α-SMA (left), and the percentage of myofibroblasts as a percentage of total fibroblasts determined (right, bar=500 μm, n=6). (**E**) *Col1a1* mRNA levels in fibroblast lysates were measured using qRT-PCR (n=6). (**F**) Col1a1 protein levels in fibroblast lysates were measured using immunoblot, and fold change quantified using densitometry with normalization to β-actin (right, n=6). Primary mouse lung fibroblasts from WT mice were incubated with bronchoalveolar lavage fluid (BALF, 20μl each mouse, 120μl total) from WT and *Fbln1c*$^{-/-}$ mice after 28 days bleomycin challenge and controls for 6 hours. (**G**) Col1a1 and pSamd3 protein in fibroblast lysates were measured using immunoblot, and (**H**) fold change quantified using densitometry with normalization to vinculin (right, n=6). Statistical differences were determined with one-way ANOVA followed by Bonferroni post-test. *P<0.05, **P<0.01, ***P<0.001, ****P<0.0001 compared to WT fibroblasts controls. †P<0.05, ††P<0.01 compared to TGF-β-stimulated WT fibroblasts controls.

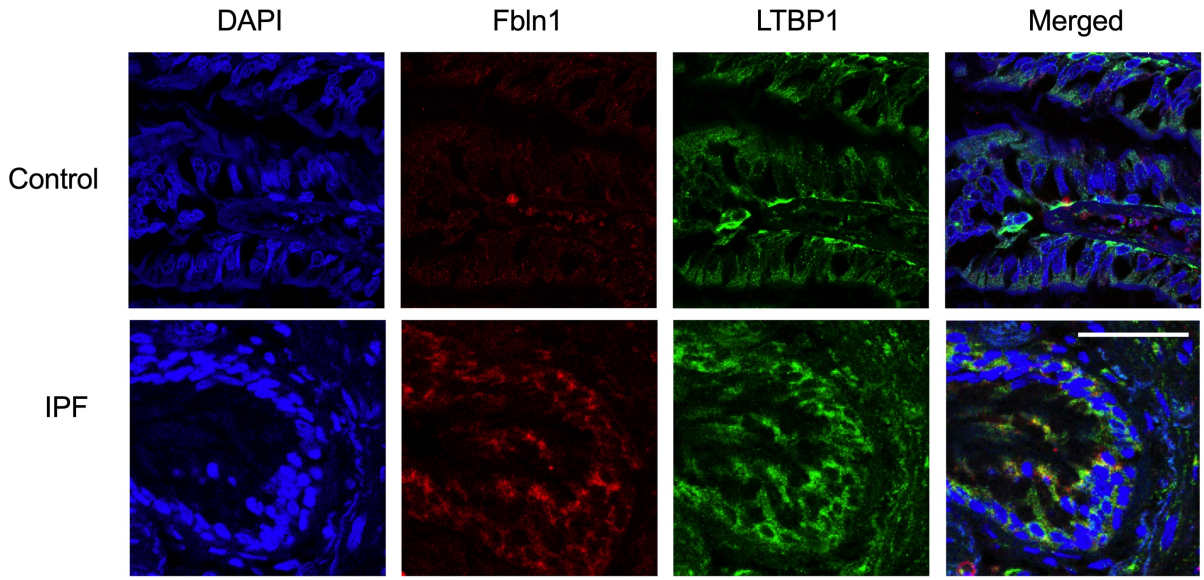

Figure 6. Fbln1 and LTBP1 colocalizes in IPF patient lungs. Lung sections were obtained from IPF patients and controls. Fbln1 (red) and LTBP1 (green) were stained using immunofluorescence, and nuclei were stained with DAPI (blue). Scale bar=50 μm.

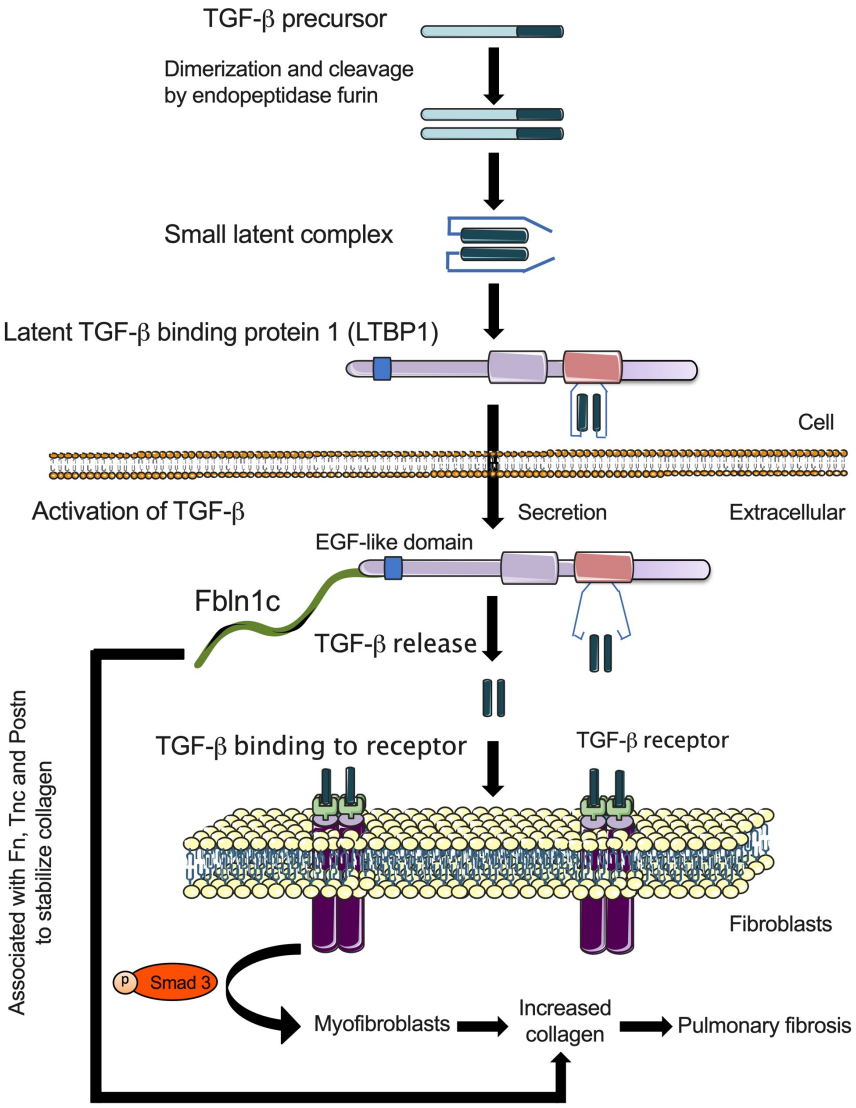

Figure 7. Proposed role of Fbln1c in pulmonary fibrosis: Fbln1c binds to latent TGF-β binding protein-1 (LTBP1) to activate TGF-β, and induce myofibroblast proliferation and collagen production. TGF-β precursors dimerize and are cleaved by the endopeptidase furin to form small latent complexes. Latent TGF-β binding protein 1 (LTBP1) binds to small latent complexes and the entire combination is secreted into the extracellular space. Fbln1c protein binds to LTBP1 likely *via* EGF-like domains on both causing the release of activated TGF-β. Fbln1c-induced activated TGF-β binds to its receptor on the surface of fibroblasts to stimulate the development and proliferation of myofibroblasts through the activity of phosphorylated Smad3 causing increased collagen production and pulmonary fibrosis. Fbln1c also associates with Fn, Tnc and Postn to stabilize the resulting collagen structure.